Synthesis and Characterization of Hypoelectronic Rhenaboranes. Analysis of the Geometric and Electronic Structures of Species Following Neither Borane nor Metal Cluster Electron-Co...

ARTICLE *in* JOURNAL OF THE AMERICAN CHEMICAL SOCIETY · APRIL 2004

Impact Factor: 12.11 · DOI: 10.1021/ja039770b · Source: PubMed

J|A|C|S
ARTICLES
Published on Web 02/25/2004

Synthesis and Characterization of Hypoelectronic Rhenaboranes. Analysis of the Geometric and Electronic Structures of Species Following Neither Borane nor Metal Cluster Electron-Counting Paradigms

Boris Le Guennic,[†] Haijun Jiao,[†,#] Samia Kahlal,[†] Jean-Yves Saillard,[†] Jean-François Halet,*[,†] Sundargopal Ghosh,[‡] Maoyu Shang,[‡] Alicia M. Beatty,[‡] Arnold L. Rheingold,[§] and Thomas P. Fehlner*[,‡]

Contribution from the Laboratoire de Chimie du Solide et Inorganique Moléculaire, UMR 6511 CNRS, Université de Rennes 1, Institut de Chimie de Rennes, Avenue du Général Leclerc, 35042 Rennes Cedex, France, Department of Chemistry and Biochemistry, University of Notre Dame, Notre Dame, Indiana 46556, and Department of Chemistry and Biochemistry, University of California San Diego, La Jolla, California 92093

Received November 24, 2003; E-mail: halet@univ-rennes1.fr; fehlner.1@nd.edu

Abstract: The reaction of $(Cp^*ReH_2)_2B_4H_4$ with monoborane leads to the sequential formation of $(Cp^*Re)_2B_nH_n$ ($n = 7-10$, **1**−**4**). These species adopt closed deltahedra with the same total connectivities as the *closo*-borane anions $[B_nH_n]^{2-}$, $n = 9-12$, but with flattened geometries rather than spherical shapes. These rhenaborane clusters are characterized by high metal coordination numbers, Re−Re cross-cluster distances within the Re−Re single bond range, and formal cluster electron counts three skeletal electron pairs short of that required for a canonical *closo*-structure of the same nuclearity. An open cluster, $(Cp^*ReH)_2B_7H_9$ (**5**), is isolated that bears the same structural relationship to *arachno*-B_9H_{15} as **1**−**4** bear to the *closo*-borane anions. Chloroborane permits the isolation of $(Cp^*ReH)_2B_5Cl_5$ (**6**), an isoelectronic chloro-analogue of known open $(Cp^*WH_2)_2B_5H_5$ and $(Cp^*Re)_2B_6H_4Cl_2$ (**7**), a triple-decker complex containing a planar, six-membered 1,2-$B_6H_4Cl_2$ ring. Both are putative five- and six-boron intermediates in the formation of **1**. Electronic structure calculations (extended Hückel and density functional theory) yield geometries in agreement with the structure determinations, large HOMO−LUMO gaps in accord with the high stabilities, and ^{11}B chemical shifts accurately reflecting the observed shifts. Analyses of the bonding in **1**−**4** reveal that the Cp*Re···Cp*Re interaction generates fragment orbitals that are able to contribute the "missing" three skeletal electron pairs required for skeletal bonding. The necessity of a Re···Re interaction for strong cluster bonding requires a borane fragment shape change to accommodate it, thereby explaining the noncanonical geometries. Application of the *debor* principle of borane chemistry to the shapes of **1**−**4** readily rationalizes the observed geometries of **5** and **6**. This evidence of the scope of transition metal fragment control of borane geometry suggests the existence of a large class of metallaboranes with structures not found in known borane or metal clusters.

Introduction

Similarities in the structural motifs that characterize boranes[1,2] and metal clusters[3] are thought to be based on common structural factors that govern the geometries and electron distributions associated with the cluster cores. The effectiveness of the cluster electron-counting rules, combined with the isolobal analogy, in explaining the vast majority of framework shapes observed to date lends considerable credence to this hypothesis.[4−10] Satisfaction in the transparent relationship of compounds of disparate stoichiometry such as $[B_6H_6]^{2-}$ and $[Ru_6(CO)_{18}]^{2-}$ (both 7 skeletal electron pair (sep), octahedral, *closo* clusters) tempts one to assume similarity in overall electronic structure. One important approximation is separation of the presumed nonbonding "t_{2g}" set of d functions of a metal fragment from the valence set used to define isolobal character; that is, Ru(CO)$_3$, like B−H, is considered a two-electron fragment with one σ and two π symmetry valence orbitals but also possesses a set of three filled "t_{2g}" metal-based orbitals in the valence

[†] Université de Rennes.
[‡] University of Notre Dame.
[§] University of California.
[#] Present address: Leibniz-Institut für Organische Katalyse, Universität Rostock e.V., Buchbinderstr. 5-6, 18055 Rostock, Germany.

(1) Lipscomb, W. N. *Boron Hydrides*; Benjamin: New York, 1963.
(2) Williams, R. E. *Inorg. Chem.* **1971**, *10*, 210.
(3) Shriver, D. F., Kaesz, H. D., Adams, R. D., Eds. *The Chemistry of Metal Cluster Complexes*; VCH: New York, 1990.
(4) Wade, K. *Electron Deficient Compounds*; Nelson: London, 1971.
(5) Wade, K. *Inorg. Nucl. Chem. Lett.* **1972**, *8*, 559.
(6) Wade, K. *New Scientist* **1974**, *62*, 615.
(7) Mingos, D. M. P. *Nature (London) Phys. Sci.* **1972**, *236*, 99.
(8) Mingos, D. M. P.; Johnston, R. L. *Struct. Bonding* **1987**, *68*, 29.
(9) Mingos, D. M. P.; Wales, D. J. *Introduction to Cluster Chemistry*; Prentice Hall: New York, 1990.
(10) Jemmis, E. D.; Balakrishnarajan, M. M.; Pancharatna, P. D. *J. Am. Chem. Soc.* **2001**, *123*, 4313.

10.1021/ja039770b CCC: $27.50

region. Woolley, in fact, argued early on against such a separation even for metal clusters formed from late transition metals with π acceptor ligands, e.g., $Ru(CO)_3$, where the approximation should be most valid.[11,12] Yet the electron-counting rules work and are demonstratively useful, particularly for the synthetic chemist. Hence, it is not a model that is in any danger of being discarded.

Metallaboranes constitute a class of compounds intermediate between borane cages on one hand and transition metal clusters on the other.[13−17] Thus, they provide a test bed for the evaluation of electronic compatibility or incompatibility of metal and borane fragments. Structures exhibited by boron-rich and metal-rich metallaboranes of the later transition metals often resemble those of the analogous borane and metal clusters. Evidence of the competition in more balanced compositions, e.g., $(CpNi)_4B_4H_4$ and $(CpCo)_4B_4H_4$,[18,19] neither of which obeys the electron-counting rules, generated much discussion.[20,21] Even in metallaborane clusters with a single transition metal fragment, examples of low sep counts, usually one less pair than predicted for the shape observed, have been reported. The structures were often found to be related to those of a *closo*-, *nido*-, or *arachno*-borane of similar nuclearity by a diamond−square−diamond (dsd) rearrangement leading to a higher coordination number at the metal center.[22] Two explanations have been offered: localization of the holes at the metal center(s) (*isocloso*[23]) or delocalization of the holes over the metal framework (*hypercloso*[24]). These views have been discussed, and examples of compounds illustrating both electronic mechanisms have been pointed out.[25−28] King has shown how utilization of the classic breakdown of a skeleton into two and three centered bonds can be used to rationalize observed *isocloso*/*hypercloso* systems.[29−31] Concurrently, a more general term, hypoelectronic, was introduced by Corbett to describe highly charged Zintl clusters with low sep counts—systems of the same generic type.[32]

The work presented below also reveals competition between main group and transition metal electronic properties. However, there is nothing subtle about the consequences of the competition. It only takes two earlier transition metals to totally dominate the cluster shapes of a homologous series of compounds containing 5−10 boron atoms. The structural motif seen is one not previously defined by either borane or metal cluster systems. Hence, the geometric and electronic structures provide an opportunity to determine the intracluster main group−transition-metal fragment interactions that lead to the observed behavior.

The development of the reaction of monocyclopentadienyl metal halides with monoboranes permits the straightforward generation of metallaboranes of the earlier transition metals for the first time.[33] Hence, we were able to access rhenaboranes, of which only a couple of examples were known previously.[34,35] Almost immediately stable $(Cp^*Re)_2B_7H_7$[36] was isolated and recognized as an analogue of $(Cp^*WH)_2B_7H_7$, produced by the pyrolysis of hydrogen-rich $Cp^*WH_3B_4H_8$.[37] These two isoelectronic nine-fragment clusters exhibited novel, uncapped closed geometries with high coordination number vertexes occupied by metal atoms and short cross-cluster metal−metal distances. Formal sep counts of 7 were considerably less than the *closo* count of 10 expected for a pure borane cluster formed from 9 BH fragments.

Upon isolation of $(Cp^*ReH_2)_2B_4H_4$, which generates $(Cp^*Re)_2B_7H_7$ on reaction with BH_3, it was clear that higher order clusters might now be accessible.[38] In the following, the synthesis and characterization of a series of dirhenium metallaboranes containing 5−10 boron atoms are described. These shapes, which lie somewhere between the highly spherical geometries of the *closo* borane dianions and the capped deltahedra found for metal clusters, pose a fundamental problem in cluster chemistry. An examination of the electronic structure of these compounds via extended Hückel and density functional methods reveals the electronic origins of the unusual shapes. Preliminary results have been communicated,[39−41] and the work has been highlighted.[42]

Results: Syntheses and Geometric Structure

$(Cp^*Re)_2B_nH_n$ (n = 7−10, 1−4). $(Cp^*ReH_2)_2B_4H_4$ reacts with BH_3·THF under mild conditions to give **1**.[38] Under more forcing conditions, a mixture of the compounds $(Cp^*Re)_2B_nH_n$ (n = 7−10) is produced. Surprisingly air stable, these compounds can be separated by thin-layer chromatography, allowing the characterization of pure materials. Molecular formulas are derived from high-resolution mass spectrometry, and the ^1H NMR confirmed the absence of hydrogen atoms other than B−H terminal and Cp* methyl hydrogens. Reactions of individual samples of pure **1**−**3** with BH_3·THF produce the higher members of the series, suggesting sequential cluster buildup rather than parallel formation from $(Cp^*ReH_2)_2B_4H_4$. Efforts to produce a compound with $n > 10$ have failed up to now.

The molecular structures of **2**−**4** in the solid state are shown in Figures 1−3, and the core geometries of **1**−**4** are compared in Chart 1. Compound **2** possesses a C_2 axis bisecting the B(1)−B(2) and B(5)−B(6) edges, making the boron atoms pairwise equivalent. However, in solution only three ^{11}B resonances (2:

(11) Woolley, R. G. *Inorg. Chem.* **1985**, *24*, 3519.
(12) Woolley, R. G. *Inorg. Chem.* **1985**, *24*, 3525.
(13) Kennedy, J. D. *Prog. Inorg. Chem.* **1984**, *32*, 519.
(14) Kennedy, J. D. *Prog. Inorg. Chem.* **1986**, *34*, 211.
(15) Grimes, R. N. In *Metal Interactions with Boron Clusters*; Grimes, R. N., Ed.; Plenum: New York, 1982; p 269.
(16) Housecroft, C. E. *Coord. Chem. Rev.* **1995**, *143*, 297.
(17) Barton, L.; Srivastava, D. K. In *Comprehensive Organometallic Chemistry II*; Abel, E., Stone, F. G. A., Wilkinson, G., Eds.; Pergamon: New York, 1995; Vol. 1.
(18) Pipal, J. R.; Grimes, R. N. *Inorg. Chem.* **1979**, *18*, 257.
(19) Bowser, J. R.; Bonny, A.; Pipal, J. R.; Grimes, R. N. *J. Am. Chem. Soc.* **1979**, *101*, 6229.
(20) Cox, D. N.; Mingos, D. M. P.; Hoffmann, R. *J. Chem. Soc., Dalton Trans.* **1981**, 1788.
(21) O'Neill, M. E.; Wade, K. *Inorg. Chem.* **1982**, *21*, 461.
(22) Kennedy, J. D. In *The Borane, Carborane, Carbocation Continuum*; Casanova, J., Ed.; Wiley: New York, 1998; p 85.
(23) Kennedy, J. D. *Inorg. Chem.* **1986**, *25*, 111.
(24) Baker, R. T. *Inorg. Chem.* **1986**, *25*, 109.
(25) Johnston, R. L.; Mingos, D. M. P. *Inorg. Chem.* **1986**, *25*, 3321.
(26) Johnston, R. L.; Mingos, D. M. P.; Sherwood, P. *New J. Chem.* **1991**, *15*, 831.
(27) Fehlner, T. P. *J. Chem. Soc., Dalton Trans.* **1998**, 1525.
(28) Weller, A. S.; Aldridge, S.; Fehlner, T. P. *Inorg. Chim. Acta* **1999**, *289*, 85.
(29) King, R. B. *Inorg. Chem.* **1999**, *38*, 5151.
(30) King, R. B.; Silaghi-Dumitrescu, I.; Kun, A. *Inorg. Chem.* **2001**, *40*, 2450.
(31) King, R. B. *Inorg. Chem.* **2001**, *40*, 2699.
(32) Sevov, S. C.; Corbett, J. D. *Inorg. Chem.* **1991**, *30*, 4875.
(33) Fehlner, T. P. *Organometallics* **2000**, *19*, 2643.
(34) Coons, D. E.; Gaines, D. F. *Inorg. Chem.* **1985**, *24*, 3774.
(35) Beckett, M. A.; Greenwood, N. N.; Kennedy, J. D.; Thornton-Pett, M. *J. Chem. Soc., Dalton Trans.* **1985**, 1119.
(36) Weller, A. S.; Shang, M.; Fehlner, T. P. *Chem. Commun.* **1998**, 1787.
(37) Weller, A. S.; Shang, M.; Fehlner, T. P. *Organometallics* **1999**, *18*, 53.
(38) Ghosh, S.; Lei, X.; Shang, M.; Fehlner, T. P. *Inorg. Chem.* **2000**, *39*, 5373.
(39) Ghosh, S.; Shang, M.; Li, Y.; Fehlner, T. P. *Angew. Chem., Int. Ed.* **2001**, *40*, 1125.
(40) Ghosh, S.; Rheingold, A. L.; Fehlner, T. P. *Chem. Commun.* **2001**, 895.
(41) Ghosh, S.; Beatty, A. M.; Fehlner, T. P. *J. Am. Chem. Soc.* **2001**, *123*, 9188.
(42) Wadepohl, H. *Angew. Chem., Int. Ed.* **2002**, *41*, 4220.

Chart 1

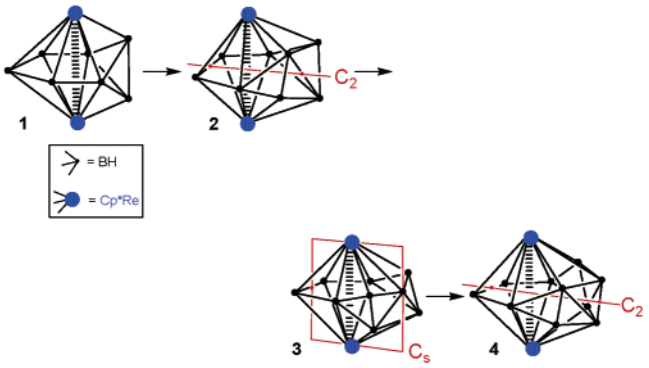

Chart 2. Heavy Red Lines Indicate the B−B Interaction Broken in the dsd Rearrangement, Whereas the Light Red Lines Indicate Those Formed

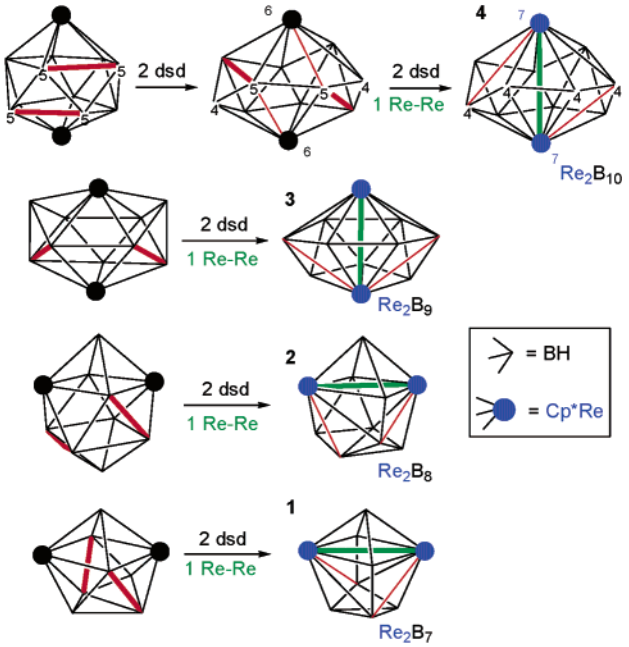

4:2) are observed from − 90 to 22 °C, suggesting accidental overlap of two signals or a low-barrier fluxional process making two pairs equivalent in solution. The electronic structure calculations (see below) show the latter to be the correct explanation. The Re atoms occupy two vertexes of connectivity 6 and d_{ReRe} = 2.8345(8) Å, which is in the range of a Re−Re single bond.[43] Compound **4** also possesses a C_2 axis bisecting the B(2)−B(3) and B(7)−B(8) edges, making the boron atoms pairwise equivalent. For **4** the observed ^{11}B resonances (2:2:2:2:2) are consistent with a static molecule in solution. The Re atoms occupy two vertexes of connectivity 7 and d_{ReRe} = 2.8192(1) Å. Compound **3** possesses a plane of symmetry passing through the Re atoms and B(5), consistent with the ^{11}B resonances (2:2:2:2:1) in solution. The Re atoms occupy one vertex of connectivity 6 and one of connectivity 7 and d_{ReRe} = 2.8604(5) Å.

As seen in Chart 2, the observed shapes of **1**−**4** are clearly different from those of the canonical deltahedra of $[B_nH_n]^{2-}$, n = 9−12.[2] Also clear is that the observed shapes can be related to the canonical ones by dsd rearrangements, as shown in Chart 2. Consequently, the total vertex connectivities (tvc) of **1**−**4** are the same as those of the canonical deltahedra of $[B_nH_n]^{2-}$ (Table 1). What is different is that the replacement of two antipodal $[BH]^-$ fragments by Cp*Re fragments generates a substantial change in the distribution of vertex connectivities. As shown in Table 1, the rhenium compounds exhibit a greater number of higher and lower connectivity vertexes than the canonical shapes: very different from the "vertex homogeneity" that governs main group cluster structures.[44] The metal atoms occupy the higher connectivity vertexes, and some of the borane fragments must, perforce, occupy lower. Consequently, the shapes of **1**−**4** are distinctly flattened along an axis containing the two vertexes of highest connectivity relative to the more spherical borane shapes. This flattening brings the metal atoms closer together, thereby introducing cross-cage Re−Re interactions.

Table 1. Comparison of the Shapes of **1**−**4** to Those of the Canonical Deltahedra in Terms of Connectivity

	number of vertexes						
connectivity	3	4	5	6	7	tvc[a]	δ[b]
1	0	5	2	2	0	42	64
$[B_9H_9]^{2-}$	0	3	6	0	0	42	−15
Δ		2	−4	2			
2	0	4	4	2	0	48	63
$[B_{10}H_{10}]^{2-}$	0	2	8	0	0	48	−2
Δ		2	−4	2			
3	0	4	5	1	1	54	43
$[B_{11}H_{11}]^{2-}$	0	2	8	1	0	54	−19
Δ		2	−3	0	1		
4	0	4	6	0	2	60	18
$[B_{12}H_{12}]^{2-}$	0	0	12	0	0	60	−16
Δ		4	−6	0	2		
5	3	3	3	0	0	36	
B_9H_{15}	4	1	4	0	0	36	

[a] Total vertex connectivity. [b] Weighted average of ^{11}B chemical shifts.

The wide range of ^{11}B NMR chemical shifts exhibited by **1**−**4** can be attributed to the presence of the metal atoms in the cage.[45−47] The shifts themselves can be assigned using the NMR shift calculations (see below), which show that the distinctive downfield resonances are associated with the low connectivity vertexes. In addition, the weighted averages of the boron resonances for the rhenaboranes can be compared to those of the corresponding borane anions (Table 1). The net downfield shift for the rhenaboranes can also be attributed to the metal atoms, and as a consequence, the average shifts upfield as the boron content of the rhenaborane increases. These geometric and spectroscopic differences are a measure of the perturbation caused by Cp*Re replacement of $[BH]^-$ in the *closo* boranes and constitute bench marks for the calculations used to investigate electronic structure.

$(Cp^*ReH)_2B_7H_9$ (5). Thermolysis of $(Cp^*ReH_2)_2B_4H_4$ at a lower temperature for a shorter time permits the isolation of a coproduct with the molecular formula $(Cp^*Re)_2B_7H_{11}$. The ^{11}B NMR spectrum exhibits three doublets in an intensity ratio of 1:4:2, consistent with a symmetric structure or a system with fluxionality. The ^{1}H NMR of **5** is somewhat unusual, but it was unraveled with a ^{1}H/^{11}B HETCOR experiment. The ^{11}B resonances at δ 98 and −7 are coupled only to terminal hydrogens, whereas that at δ 28 is linked to three: a terminal

(43) Poli, R.; Wilkinson, G.; Moetevailli, M.; Hursthouse, M. B. *J. Chem. Soc., Dalton Trans.* **1985**, 931.
(44) Williams, R. E. In *The Borane, Carborane, Carbocation Continuum*; Casanova, J., Ed.; Wiley-Interscience: New York, 1997; p 3.
(45) Rath, N. P.; Fehlner, T. P. *J. Am. Chem. Soc.* **1988**, *110*, 5345.
(46) Fehlner, T. P.; Czech, P. T.; Fenske, R. F. *Inorg. Chem.* **1990**, *29*, 3103.
(47) Fehlner, T. P. *Collect. Czech. Chem. Commun.* **1999**, *64*, 767.

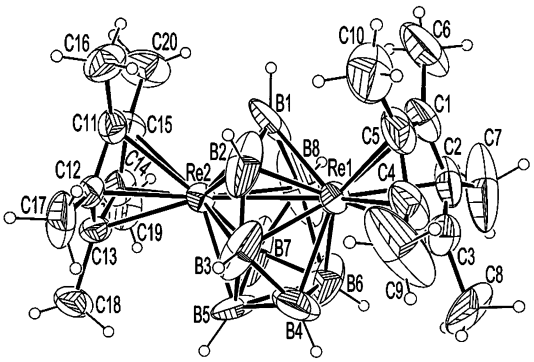

Figure 1. Molecular structure of $(Cp^*Re)_2B_8H_8$ (**2**). Selected bond lengths (Å): Re(1)−B(2) 2.04(3), Re(1)−B(1) 2.09(3), Re(1)−B(8) 2.16(2), Re(1)−B(4) 2.211(19), Re(1)−B(3) 2.27(3), Re(1)−B(6) 2.33(3), Re(1)−Re(2) 2.8345(8), Re(2)−B(2) 2.05(2), Re(2)−B(1) 2.076(18), Re(2)−B(7) 2.19(2), Re(2)−B(3) 2.21(2), Re(2)−B(5) 2.31(2), Re(2)−B(8) 2.35(3), B(1)−B(2) 1.82(5), B(1)−B(8) 1.94(5), B(2)−B(3) 1.65(4), B(3)−B(4) 1.76(5), B(3)−B(5) 2.18(5), B(4)−B(5) 1.55(3), B(4)−B(6) 1.74(4), B(5)−B(7) 1.89(5), B(5)−B(6) 2.03(5), B(6)−B(7) 1.73(4), B(6)−B(8) 2.02(5), B(7)−B(8) 1.66(5).

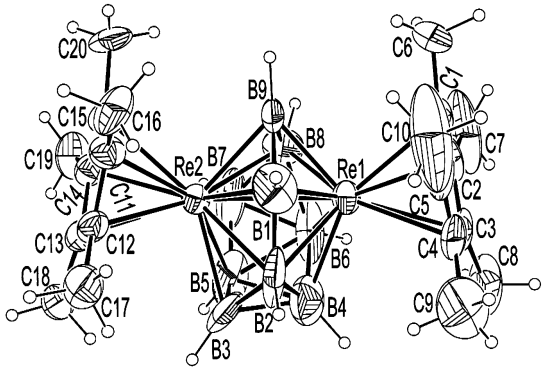

Figure 2. Molecular structure of $(Cp^*Re)_2B_9H_9$ (**3**). Selected bond lengths (Å): Re(1)−B(1) 1.982(14), Re(1)−B(9) 2.075(12), Re(1)−B(8) 2.187(14), Re(1)−B(6) 2.209(12), Re(1)−B(4) 2.212(14), Re(1)−B(2) 2.216(15), Re(1)−Re(2) 2.8604(5), Re(2)−B(9) 2.165(11), Re(2)−B(1) 2.198(11), Re(2)−B(3) 2.215(13), Re(2)−B(7) 2.217(14), Re(2)−B(5) 2.299(16), Re(2)−B(2) 2.336(11), Re(2)−B(8) 2.402(13), B(1)−B(2) 1.70(2), B(1)−B(9) 1.869(18), B(2)−B(3) 1.70(2), B(2)−B(4) 1.83(3), B(3)−B(5) 1.55(2), B(3)−B(4) 1.63(2), B(4)−B(6) 1.86(2), B(4)−B(5) 1.858(18), B(5)−B(7) 1.67(2), B(5)−B(6) 1.86(2), B(6)−B(7) 1.736(19), B(6)−B(8) 1.82(2), B(7)−B(8) 1.646(19), B(8)−B(9) 1.794(17).

BH at δ 0.7, BHB at 0.04, and ReHB at −10.8. Other than thermal decoupling of the BH resonances, the ^{1}H NMR spectrum was independent of temperature down to −85 °C.

The molecular geometry in the solid state shows an open core structure (Figure 4) and, ignoring the bridging hydrogen atoms, has three types of boron sites in the ratio of 1:2:4. Consistent with the discussion above, the signal of intensity 1 at δ 98 can be assigned to the unique four-connect boron and the signal of intensity 2 at −7 to the two five-connect borons. The remaining signal of intensity 4 must be associated with the borons lying on the open face of **5**. The two BHB and two ReHB hydrogens can be placed as shown in either Chart 3a or 3b. The former constitutes a static structure, whereas in the latter the ReHB hydrogens must flip back and forth between the two adjacent boron atoms rapidly on the NMR time scale: a fluxional process with precedent in metallaborane chemistry.[48] The Re−Re distance of **5** is about 0.15 Å longer than found in **1**−**4**; however, it is nearly the same as the W−W distance in closed $(Cp^*WH)_2B_7H_7$, which also contains bridging hydrogen atoms.[37]

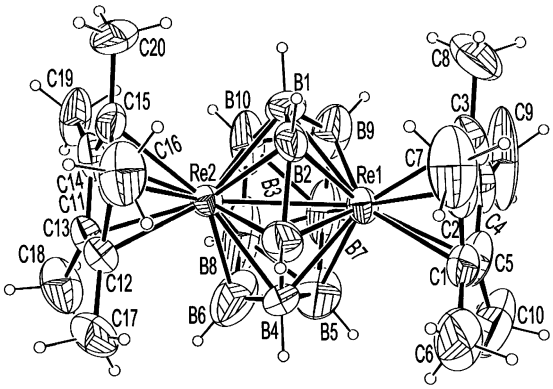

Figure 3. Molecular structure of $(Cp^*Re)_2B_{10}H_{10}$ (**4**). Selected bond lengths (Å): Re(1)−B(2) 2.120(14), Re(1)−B(3) 2.185(15), Re(1)−B(4) 2.248(14), Re(1)−B(9) 2.268(17), Re(1)−B(1) 2.271(18), Re(1)−B(5) 2.272(17), Re(1)−B(7) 2.408(18), Re(2)−B(3) 2.131(13), Re(2)−B(6) 2.18(2), Re(2)−B(2) 2.190(13), Re(2)−B(4) 2.226(15), Re(2)−B(1) 2.226(14), Re(2)−B(8) 2.31(2), B(1)−B(2) 1.67(2), B(1)−B(9) 1.72(3), B(1)−B(10) 1.83(3), B(2)−B(3) 1.747(19), B(3)−B(4) 1.67(3), B(4)−B(6) 1.58(3), B(4)−B(5) 1.74(3), B(5)−B(6) 1.59(3), B(5)−B(7) 1.78(3), B(5)−B(8) 1.93(3), B(6)−B(8) 1.52(4), B(7)−B(9) 1.65(3), B(7)−B(8) 1.67(3), B(7)−B(10) 2.02(3), B(8)−B(10) 1.79(4), B(9)−B(10) 1.62(2).

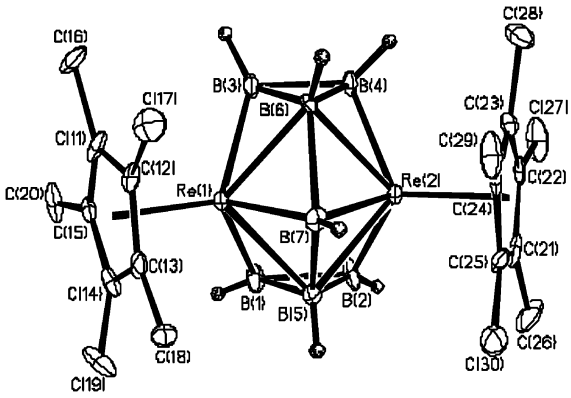

Figure 4. Molecular structure of $(Cp^*Re)_2B_7H_{11}$ (**5**). Selected bond distances (Å) for one of two independent but chemically equivalent molecules: Re(1)−Re(2) 2.9744(5), Re(1)−B(1) 2.216(13), Re(1)−B(3) 2.221(13), Re(1)−B(5) 2.241(12), Re(1)−B(6) 2.271(11), Re(2)−B(2) 2.227(12), Re(2)−B(4) 2.211(12), Re(2)−B(5) 2.236(12), Re(2)−B(6) 2.258(13), Re(2)−B(7) 2.091(12), B(1)−B(2) 1.753(17), B(1)−B(5) 1.728(17), B(2)−B(5) 1.736(19), B(3)−B(4) 1.747(16), B(4)−B(6) 1.734(18), B(5)−B(7) 2.012(18), B(6)−B(7) 2.044(17).

Chart 3

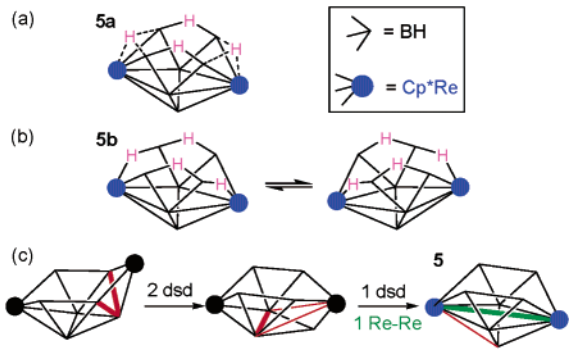

The shape of **5** is not anticipated based on the canonical borane *nido* or *arachno* structures. However, it is related to these structures in the same manner as **1**−**4** are related to the *closo*

(48) Shore, S. G.; Raganini, D.; Smith, R. L.; Cottrell, C. E.; Fehlner, T. P. *Inorg. Chem.* **1979**, *18*, 670.

borane structures. **5** has a framework with a tvc = 36 and the canonical nine fragment *closo*, *nido*, and *arachno* shapes have tvc's of 42, 38, and 36, respectively.[44] Thus, **5** is classified as a 9 sep *arachno* analogue of a 12 sep canonical *arachno* borane, e.g., B_9H_{15}. As shown in Chart 3c, they are related by dsd rearrangements, and as shown in Table 1, the rhenaborane possesses a less symmetric distribution of vertex connectivities. The composition of **5** suggests that it may lie on the reaction pathway to **1**; however the pyrolysis of **5** did not yield **1**. H_2 elimination from **5** must involve a substantial barrier.

Identification of Intermediates. Additional information on the origin of **1**−**5** was sought in a search for the five and six boron atom intermediates expected if the generation of **1** from $(Cp^*ReH_2)_2B_4H_4$ is a stepwise process similar to those already known for other metallaboranes.[49,50] In addition to mechanistic value, this information is pertinent to the electronic structure problem posed by compounds **1**−**5**.

If Re_2B_5 and Re_2B_6 intermediates are formed in the reaction with borane, their rate of conversion to higher products or to decomposition products must be faster than formation from $(Cp^*ReH_2)_2B_4H_4$. Previously we found that chloromonoboranes, $BH_2Cl{\cdot}SMe_2$ and $BHCl_2{\cdot}SMe_2$, are effective in inserting borane fragments into metallaboranes with different rates than found for $BH_3{\cdot}THF$.[51,52] Although we had no way of knowing whether rates would be changed in a helpful direction, the possibility of generating higher stationary state concentrations of intermediates was there. The price paid is Cl incorporation either directly or via H/Cl exchange. However, clean reactions were of lower importance in a search for intermediates. Three were characterized and provide important additional information.

$(Cp^*ReH)_2B_5Cl_5$ (6). A five-boron species with composition $(Cp^*ReH)_2B_5Cl_5$ exhibits three signals in the ^{11}B NMR in an intensity ratio of 2:2:1 with no large coupling to protons. The species, perchlorinated in the terminal positions, shows single Cp* methyl and Re−H signals in the ^1H NMR spectrum in a ratio of 15:1. The molecular structure in the solid state is shown in Figure 5, where this compound is seen to be a cluster analogue of $Cp^*_2M_2B_5H_9$, M = Cr, Mo, W,[37,52,53] with which it is isoelectronic (Chart 4). The Re−H hydrogen atoms were not located, but the ^1H NMR spectrum shows rhenium hydride resonances with a Cp*:ReH ratio of 1:1. The compound must be fluxional in the same sense as **5**.

Compound **6** constitutes the first example of a dimetallaborane fully chlorinated at boron and is interesting in its own right. But it is of more importance in a mechanistic sense. Unsaturated $(Cp^*Cr)_2B_4H_8$ adds borane to form $(Cp^*Cr)_2B_5H_9$.[52] Hence, it seems clear that $(Cp^*ReH_2)_2B_4H_4$ adds borane to yield $(Cp^*ReH)_2B_5H_5$ on the way to **1** (Chart 5). Of course a parallel pathway cannot be eliminated, but as stepwise borane addition has been previously observed in M_2B_n systems for n = 1−4 and 7−9, a sequential path is probable.[54] The hydrogen derivative of **6** also is a reasonable intermediate in the formation of **5** (Chart 5).

(49) Lei, X.; Shang, M.; Fehlner, T. P. *J. Am. Chem. Soc.* **1999**, *121*, 1275.
(50) Lei, X.; Bandyopadhyay, A. K.; Shang, M.; Fehlner, T. P. *Organometallics* **1999**, *18*, 2294.
(51) Hong, F.-E.; Eigenbrot, C. W.; Fehlner, T. P. *J. Am. Chem. Soc.* **1989**, *111*, 949.
(52) Aldridge, S.; Hashimoto, H.; Kawamura, K.; Shang, M.; Fehlner, T. P. *Inorg. Chem.* **1998**, *37*, 928.
(53) Aldridge, S.; Shang, M.; Fehlner, T. P. *J. Am. Chem. Soc.* **1998**, *120*, 2586.
(54) Lei, X.; Shang, M.; Fehlner, T. P. *Chem. Eur. J.* **2000**, *6*, 2653.

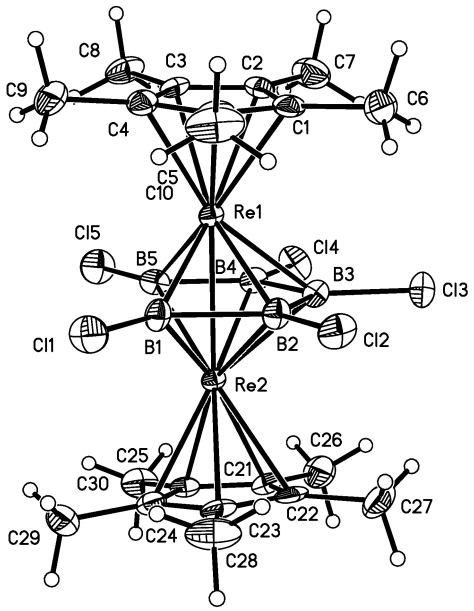

Figure 5. Molecular structure of $(Cp^*ReH)_2B_5Cl_5$ (**6**). Selected bond lengths (Å): Re(1)−B(1) 2.118(6), Re(1)−B(2) 2.171(6), Re(1)−B(3) 2.214(6), Re(1)−B(4) 2.231(6), Re(1)−C(3) 2.241(5), Re(1)−B(5) 2.268(6), Re(1)−Re(2) 2.7641(3), Re(2)−B(1) 2.120(7), Re(2)−B(2) 2.162(6), Re(2)−B(3) 2.220(6), Re(2)−B(4) 2.227(6), Re(2)−B(5) 2.275(6), Re(2)−C(23) 2.316(5), Cl(1)−B(1) 1.764(6), Cl(2)−B(2) 1.778(6), Cl(3)−B(3) 1.788(6), Cl(4)−B(4) 1.803(6), Cl(5)−B(5) 1.794(6), B(1)−B(2) 1.878-(8), B(2)−B(3) 1.730(8), B(3)−B(4) 1.677(8), B(4)−B(5) 1.707(8).

Chart 4

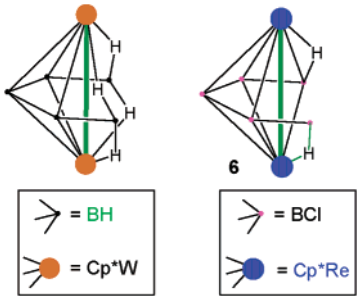

Chart 5. Green Lines Correspond to the New Bonding Interactions Generated by the Inserted BH Fragment

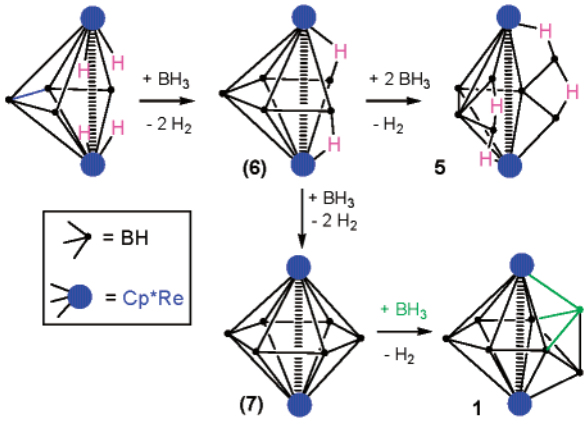

$(Cp^*Re)_2B_6H_4Cl_2$ (7). A second compound with molecular formula $(Cp^*Re)_2B_6H_4Cl_2$ exhibits three types of boron environments in a 1:1:1 ratio, only two of which show coupling to terminal hydrogen atoms. The ^1H NMR reveals equivalent Cp* ligands and no metal hydrides or bridging hydrogen atoms. The

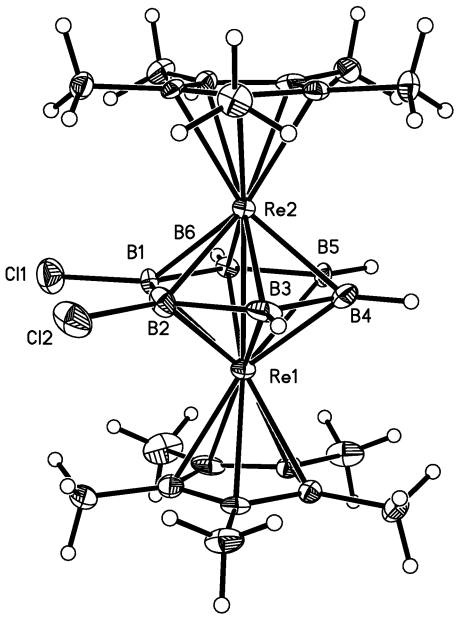

Figure 6. Molecular structure of $(Cp^*Re)_2B_6H_4Cl_2$ (**7**). Selected bond lengths (Å) from one independent molecule: Re(1)−B(2) 2.145(12), Re(1)−B(1) 2.169(10), Re(1)−B(4) 2.192(11), Re(1)−B(5) 2.200(11), Re(1)−B(6) 2.229(10), Re(1)−B(3) 2.246(13), Re(1)−Re(2) 2.6887(5), Re(2)−B(2) 2.153(12), Re(2)−B(5) 2.161(10), Re(2)−B(4) 2.169(11), Re(2)−B(1) 2.173(10), Re(2)−B(6) 2.179(10), Re(2)−B(3) 2.231(12), Cl(1)−B(1) 1.746(10), Cl(2)−B(2) 1.787(12), B(1)−B(6) 1.710(15), B(1)−B(2) 1.780(16), B(2)−B(3) 1.700(18), B(3)−B(4) 1.732(19), B(4)−B(5) 1.701(17), B(5)−B(6) 1.732(15).

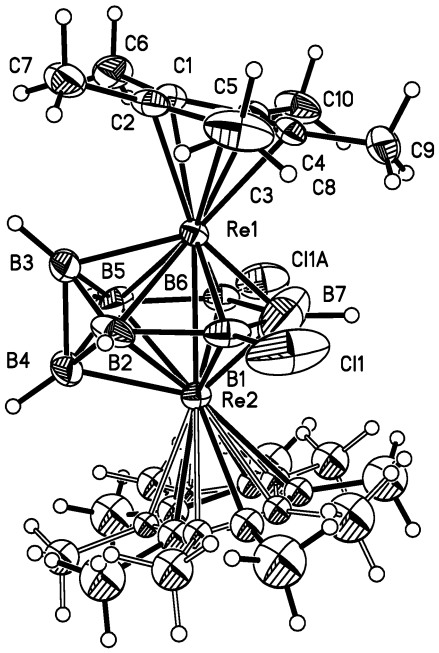

Figure 7. Molecular structure of $(Cp^*Re)_2B_7H_6Cl$ (**8**) showing modeled disorder in the Cl atom and one Cp* ligand. Selected bond lengths (Å): Re(1)−B(7) 1.978(17), Re(1)−B(1) 2.091(8), Re(1)−B(6) 2.129(8), Re(1)−B(3) 2.151(7), Re(1)−B(5) 2.269(8), Re(1)−B(2) 2.286(7), Re(1)−Re(2) 2.6895(4), Re(2)−B(7) 1.96(2), Re(2)−B(1) 2.100(9), Re(2)−B(6) 2.109(8), Re(2)−B(4) 2.160(10), Re(2)−B(5) 2.259(8), Re(2)−B(2) 2.314(7), Cl(1)−B(1) 1.791(10), Cl(1A)-B(6) 1.630(19), B(6)−B(5) 1.801(13), B(6)−B(7) 1.93(2), B(7)−B(1) 1.73(3), B(1)−B(2) 1.795(14), B(2)−B(4) 1.731(13), B(2)−B(3) 1.7354, B(3)−B(4) 1.690(12), B(3)−B(5) 1.738(12), B(4)−B(5) 1.759(16).

molecular structure of **7** is shown in Figure 6, where it is seen to be fully consistent with the solution spectroscopic data. The average Re−Re distance of 2.6889(5) Å is shorter than that found in **1**−**5** but longer than that expected for a Re−Re double bond.[55] The borane fragment is a planar, six-membered ring with two adjacent boron atoms substituted by chlorine atoms of structure similar to a dichromium compound containing a planar B_4C_2 ring.[56] Hence, **7** is seen to be a 24 valence electron triple-decker complex and an interesting new member of a class of compounds exhibiting a wide variation in electron counts.[57,58]

The hydrogen analogue of **7**, in turn, is a likely intermediate in the formation of **1** from addition of BH_3·THF to $(Cp^*ReH_2)_2B_4H_4$. Again a parallel reaction cannot be ruled out, but simple insertion of a BH fragment into a Re−B edge of **7** leads directly to **1** (Chart 5) in the same manner that **1** is converted into **2**, then **3**, etc. It is relevant that the reaction of $Co_2(CO)_8$ with $(Cp^*ReH_2)_2B_4H_4$ leads to the formation of $\{Cp^*Re\}_2\{\mu\text{-}\eta^6\text{:}\eta^6\text{-}1,2\text{-}B_4H_4Co_2(CO)_5\}$, which is an isolobal metal analogue of $(Cp^*Re)_2B_6H_6$.[59]

$(Cp^*Re)_2B_7H_6Cl$ (8). The identification of $(Cp^*Re)_2B_7H_6Cl$ (**8**) is based solely on a solid state structure determination of a crystal selected from a mixture of **8** and **1** (by ^{11}B NMR). The molecular structure of **8** is shown in Figure 7, where it is seen to be a monochlorinated derivative of **1**. As expected, the distances and angles are similar to those found in **1**. The observation of **1** and **8** in the dichloroborane reaction is important mechanistically, as it shows that the reaction of dichloroborane with $(Cp^*ReH_2)_2B_4H_4$ proceeds, at least in part, in the same manner as with borane itself.

Results: Electronic Structure

The answer to the problem posed concerning the role of the rhenium fragments in determining the observed framework shapes resides in the electronic structures of these species. Quantum chemistry provides the tools for understanding the relationship between geometry and bonding in the hypoelectronic compounds **1**−**8**. Hence, theoretical calculations using the extended Hückel theory (EHT) and density functional theory (DFT) methods were carried out on the model complexes **1H**−**8H** with Cp ligands instead of Cp* ligands. Calculated properties include (i) the geometries of the clusters, (ii) energetics, and (iii) magnetic properties. These establish the validity of the methods as well as complete the characterization of the compounds. Finally, the model of the electronic structure that develops permits the electronic origins of the novel observed structures to be investigated.

Geometries. The related compounds $(Cp^*Re)_2B_nX_n$ (n = 7−10, **1**−**4**), $(Cp^*Re)_2B_6H_4Cl_2$ (**7**), and $(Cp^*Re)_2B_7H_6Cl$ (**8**) were studied first. Pertinent DFT optimized bond distances for the corresponding models **1H**−**4H**, **7H**, and **8H** of symmetry C_{2v}, C_2, C_s, C_2, C_2, and C_s, respectively, are given in Table 2. Satisfactory agreement is found between these computed bond lengths and those of the crystallographically characterized complexes **1**−**4**, **7**, and **8** (see above). The observed deviation between the computed distances and the experimental values

(55) Cotton, F. A.; Walton, R. A. *Multiple Bonds Between Metal Atoms*; Wiley: New York, 1982.
(56) Kawamura, K.; Shang, M.; Wiest, O.; Fehlner, T. P. *Inorg. Chem.* **1998**, *37*, 608.
(57) Herberich, G. E. In *Comprehensive Organometallic Chemistry II*; Abel, E., Stone, F. G. A., Wilkinson, G., Eds.; Pergamon Press: Oxford, 1995; Vol. 1, p 197.
(58) Jemmis, E. D.; Reddy, A. C. *Organometallics* **1988**, *7*, 1561.
(59) Ghosh, S.; Shang, M.; Fehlner, T. P. *J. Am. Chem. Soc.* **1999**, *121*, 7451.

Table 2. Selected Optimized Bond Lengths (Å), HOMO−LUMO Gaps (ΔE, eV), and Vertical Ionization Potentials (IP_{Vert}, eV) for the Model Complexes $(CpRe)_2B_nH_n$ (n = 7−10, **1H**−**4H**), $(CpRe)_2B_6H_4Cl_2$, **7H**, and $(CpRe)_2B_7H_6Cl$, **8H**

	1H	2H	3H	4H	7H	8H
			Optimized Bond Lengths			
Re_1-Re_2	2.817	2.882	2.889	2.860	2.714	2.809
Re_1-B_1	2.121	2.154	2.106	2.300		2.155
Re_1-B_2	2.163	2.080	2.236	2.152	2.188	2.311
Re_1-B_3		2.313		2.252	2.210	2.182
Re_1-B_4	2.304	2.128	2.267	2.274	2.213	
Re_1-B_5				2.389		2.306
Re_1-B_6	2.165	2.305				2.170
Re_1-B_7				2.430		2.123
Re_1-B_8		2.192				
Re_1-B_9				2.238		
Re_2-B_1			2.205			
Re_2-B_2			2.366			
Re_2-B_3			2.284			
Re_2-B_5			2.400			
B_1-B_1			1.935			
B_1-B_2	1.882	2.000	1.805	1.751	1.767	1.824
B_1-B_7						1.900
B_2-B_3		1.885	1.710	1.781	1.741	1.769
B_2-B_4	1.809		1.805			
B_3-B_4		1.771	1.756		1.721	1.716
B_3-B_5		1.809	1.688			1.771
B_4-B_4			1.943			
B_4-B_5		1.729	1.862	1.827	1.725	
B_4-B_6	1.772	1.805		1.722		
B_5-B_6		1.940		1.748		1.805
B_5-B_7				1.794		
B_5-B_8				1.817		
B_6-B_7	1.718					1.897
B_6-B_8				1.691		
B_7-B_8				1.754		
			HOMO−LUMO Gaps			
ΔE	2.67	2.45	2.38	2.72	2.31	2.81
			Vertical Ionization Potentials			
IP_{vert}	7.60	7.37	7.40	7.48	7.52	7.82

may be ascribed to some extent to the replacement of the Cp* ligands by Cp ligands used to reduce computational effort. In the case of $(CpRe)_2B_7H_7$ (**1H**) for instance the computed Re−Re distance is 0.029 Å longer than that experimentally observed in **1**. The computed Re−B separations are ≤0.07 Å longer than the experimental ones. Slightly larger deviations, ca. 0.08−0.10 Å on average, are observed for the B−B distances, but still within the experimental uncertainties in the measured B−B distances. Comparable deviations are observed for the other complexes. Such deviations reflect in part the fact that the B−B separations in electron-poor clusters are quite flexible and can vary up to 0.3 Å almost without any energy cost. In accord with the measured structure parameters, the computed Re−Re distances in $(CpRe)_2B_nX_n$ are nearly invariant with n for n > 8, whereas the B−B bond distances increase slightly on average as n increases.

The rather good agreement between computed and experimental bond lengths in the species $(Cp^*Re)_2B_nX_n$ permits the computational method to be used to corroborate the structure characterizations of those rhenaboranes containing hydrogen atoms not located in the X-ray structure determination and/or in compounds possessing possible isomers further complicated by fluxional behavior, e.g., the compounds $(Cp^*ReH)_2B_7H_9$ (**5**) and $(Cp^*ReH)_2B_5Cl_5$ (**6**).

In **5** the four bridging hydrogen atoms can be placed on the metal−boron skeleton in two ways. The proton NMR shows that two hydrogen atoms bridge B−B bonds (B(1)−B(2) and B(3)−B(4)), whereas the two others either bridge triangular ReB_2 faces, lying in the plane of symmetry containing the two Re atoms and the unique B atom (isomer **5a** of C_{2v} symmetry), or bridge two of the four Re−B edges on the hexagonal opening (isomer **5b** of C_2 symmetry) (Chart 3). Computations carried out on either model **5aH** or **5bH** produce Re−Re, Re−B, and B−B bond lengths similar to the corresponding distances measured for **5** (Table 2). Neither isomer is favored over the other on geometrical and energetic parameters alone. In both isomers, B−H bond lengths of about 1.34 Å are computed for the hydrogen atoms bridging B−B bonds. For the Re−H−B bridges, the Re−H distances are comparable (1.688 and 1.729 Å in **5aH** and **5bH**, respectively), while the B−H distances differ (1.874 and 1.467 Å in **5aH** and **5bH**, respectively). Despite these geometric differences, with only ∼2 kcal/mol difference in energy in favor of **5bH**, it is probable that the hydrogen atoms bridge Re−B bonds and flip back and forth between B(2) and B(4) and B(1) and B(3) rapidly on the NMR time scale.

NMR data suggest that the two hydrogen atoms in the compound $(Cp^*ReH)_2B_5Cl_5$ (**6**) bridge two Re−B bonds of the open face. Consequently, two isomeric forms, either *cis* or *trans* with respect to the plane of symmetry containing the two Re atoms and the unique boron atom B(3), can be proposed. The two corresponding models **6aH** and **6bH** of C_s (Re(1)−H−B(1) and Re(2)−H−B(5)) and C_2 (Re(1)−H−B(1) and Re(2)−H−B(1)) symmetry, respectively, were computed. The Re−Re distances found are similar in these two model complexes (2.796 vs 2.797 Å) and only 0.03 Å longer than the experimental value (2.7641(3) Å). Interestingly, the Re−H and B−H bond lengths slightly differ from one isomer to the other, with longer Re−H and shorter B−H separations in isomer **6aH** (1.751 vs 1.732 Å and 1.403 vs 1.423 Å in **6aH** and **6bH**, respectively). Once again the two arrangements are nearly isoenergetic (less than 2 kcal/mol in favor of isomer **6bH**), consistent with fluxional behavior in solution.

Electronic Structures and MO Analysis. DFT molecular orbital diagrams of the model compounds **1H**−**4H** and **7H** are shown in Figure 8. For each compound, a large energy gap (>2 eV) separates the occupied MO set from the vacant orbital set (Table 2). This is consistent with the stability of these dirhenaboranes. Contrary to the behavior of, for example, linear carbon chains, there is no decrease of the HOMO−LUMO gap as the number of boron atoms increases from 6 to 10.[60] The HOMO−LUMO gaps are rather large and nearly the same for every value of n. In fact, this has been observed before for deltahedral boranes,[61] and the underlying reason may be associated with small changes in the connectivity of boron and metal atoms in the series.

Large HOMO−LUMO gaps are also computed for **5H** and **6H** (regardless of the isomeric arrangements *a* or *b*, see Table 3), which is again consistent with the high apparent stabilities. The composition of the orbitals located in the HOMO region (Supporting Information) reflects strong delocalization over the whole Re_2B_n skeleton and lies in a small energy range. Note that the metal character of the HOMO varies substantially from ca. 30% (31% in **4H** and **6H**, 28% in **7H**) to ca. 70% (70% in **1H** and **8H**, 71% in **2H**, 64% in **3H** and **5H**).

Ionization Potentials. A more realistic indicator of cage stability is ionization potential (IP) energy. Vertical and adiabatic

(60) Albright, T. A.; Burdett, J. K.; Whangbo, H.-H. *Orbital Interactions in Chemistry*; Wiley: New York, 1985.
(61) McKee, M. L.; Wang, Z.-X.; Schleyer, P. v. R. *J. Am. Chem. Soc.* **2000**, *122*, 4781.

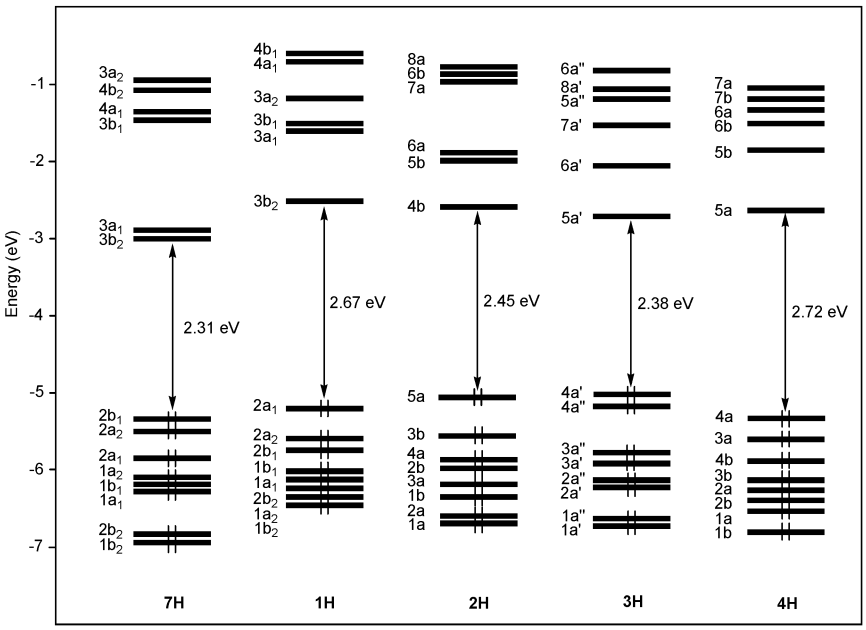

Figure 8. DFT orbital diagrams for the model complexes $(CpRe)_2B_nH_n$ ($n = 7-10$, **1H**−**4H**) and $(CpRe)_2B_6H_4Cl_2$, **7H**.

Table 3. Selected Optimized Bond Lengths (Å), Relative Energies (E, eV), HOMO−LUMO Gaps (ΔE, eV), and Vertical Ionization Potentials (IP_{vert}, eV) for the Model Complexes $(CpReH)_2B_7H_9$, **5H**, and $(CpReH)_2B_5Cl_5$, **6H**

	5aH	5bH	6aH	6bH
		Optimized Bond Lengths		
Re_1-Re_2	2.988	2.997	2.796	2.797
Re_1-B_1	2.255	2.243	2.291	2.143
Re_1-B_2			2.253	2.234
Re_1-B_3		2.288	2.221	2.220
Re_1-B_4			2.174	2.207
Re_1-B_5	2.269	2.294	2.125	2.250
Re_1-B_6		2.238		
Re_1-B_7	2.089	2.090		
B_1-B_2	1.720	1.730	1.702	1.761
B_1-B_5	1.735	1.729		
B_1-B_7				
B_2-B_3			1.689	1.701
B_3-B_4			1.722	
B_3-B_6		1.748		
B_4-B_5			1.872	
B_5-B_7	2.062	2.065		
B_6-B_7				
Re−H	1.688	1.729	1.751	1.732
B−H	1.334[a]/1.874[b]	1.338[a]/1.467[b]	1.403	1.423
		Relative Energies		
E	0.09	0.00	0.00	0.08
		HOMO−LUMO Gaps		
ΔE	3.15	2.86	1.86	1.47
		Vertical Ionization Potentials		
IP_{vert}	7.29	7.03	7.05	6.82

[a] H atoms bridging B−B bonds. [b] H atoms bridging Re−B bonds.

first IPs for one-electron loss were computed for the $(CpRe)_2B_nX_n$ series ($n = 6-10$) and are plotted in Figure 9. IP values above 7 eV are consistent with observed high stability. The adiabatic curve is a few tenths of an eV lower in energy, as expected, and although the two curves do not track each other exactly, the conclusion is the same.

NMR Chemical Shifts. The effectiveness of DFT at handling NMR calculations on ^{11}B NMR chemical shifts has been demonstrated by studies on many boranes and heteroboranes.[62−68] The accuracy has been sufficient to resolve a number of outstanding problems in the field. The application of the approach to metallaboranes is a challenge, particularly for the

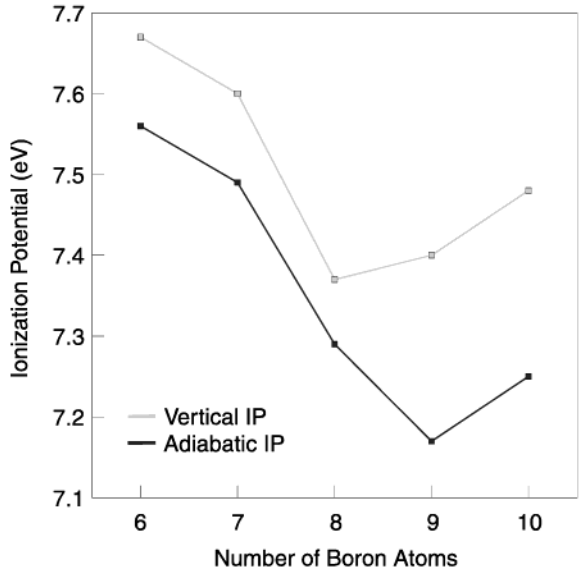

Figure 9. Plot of the first vertical and adiabatic ionization potential (IP, eV) for the model complexes $(CpRe)_2B_nH_n$ ($n = 6-10$, **1H**−**4H**, **7′H**).

heavier transition metals such as Re, where relativistic corrections are important. In addition, the presence or absence of bridging hydrogen atoms, the number of direct metal−boron bonds, the metal identity, and coordination number are all important in determining the boron chemical shifts.[47] Indeed, accuracy of chemical shift calculations depends on the accuracy of the geometry, as it is known that small changes in bond lengths or angles may lead to significant deviations in the

(62) Bühl, M.; Schleyer, P. v. R. *Angew Chem., Int. Ed. Engl.* **1990**, *29*, 886.
(63) Bühl, M.; Schleyer, P. v. R. *J. Am. Chem. Soc.* **1992**, *114*, 477.
(64) Bühl, M.; Gauss, J.; Hofmann, M.; Schleyer, P. v. R. *J. Am. Chem. Soc.* **1994**, *115*, 12385.
(65) Bausch, J. W.; Prakash, G. K. S.; Bühl, M.; Schleyer, P. v. R.; Williams, R. E. *Inorg. Chem.* **1992**, *31*, 3060.
(66) Onak, T.; Tran, D.; Tseng, J.; Diaz, M.; Arias, J.; Herrera, S. *J. Am. Chem. Soc.* **1993**, *115*, 9210.
(67) Onak, T.; Tseng, J.; Diaz, M.; Tran, D.; Arias, J.; Herrera, S.; Brown, D. *Inorg. Chem.* **1993**, *32*, 487.
(68) Shedlow, A. M.; Kadlecek, D. E.; Clapper, J. C.; Rathmill, S. E.; Carroll, P. J.; Sneddon, L. G. *J. Am. Chem. Soc.* **2003**, *125*, 200.

Table 4. Calculated ^{11}B and ^{1}H NMR Chemical Shifts (δ, ppm) for $(CpRe)_2B_nH_n$ ($n = 7-10$, **1H**−**4H**), $(CpReH)_2B_7H_9$, **5H**, $(CpReH)_2B_5Cl_5$, **6H**, $(CpRe)_2B_6H_4Cl_2$, **7H**, and $(CpRe)_2B_7H_6Cl$, **8H**, Compared with the Corresponding Experimental Chemical Shifts

	^{11}B NMR			^{1}H NMR		
	atom	exptl	calcd	atom	exptl	calcd
1H	B(1)	101.7	83.2	H(1)	10.1	6.1
	B(2), B(3)	85.6	66.9	H(2), H(3)	11.2	7.0
	B(6), B(7)	82.1	61.8	H(6), H(7)	8.6	5.4
	B(4), B(5)	3.6	0.9	H(4), H(5)	−0.1	2.2
2H	B(1), B(2)	97.9	78.3	H(1), H(2)	9.9	6.2
	B(5), B(6), B(4), B(7)	65.8[a]	14.5 106.7	H(5), H(6), H(4), H(7)	9.0[a]	2.5 9.14
	B(3), B(8)	21.9	14.0	H(3), H(8)	1.9	2.1
3H	B(1), B(9)	94.1	75.6	H(1), H(9)	11.2	10.8
	B(3), B(7)	74.2	71.1	H(3), H(7)	10.2	7.7
	B(4), B(6)	35.5	32.7	H(4), H(6)	8.5	3.7
	B(2), B(8)	1.1	−6.7	H(2), H(8)	−0.1	−0.3
	B(5)	−28.7	−34.9	H(5)	−2.3	2.9
4H	B(6), B(9)	60.0	39.3	H(6), H(9)	8.6	6.1
	B(2), B(3)	50.4	36.4	H(2), H(3)	6.8	4.6
	B(1), B(4)	16.1	28.0	H(1), H(4)	6.0	3.5
	B(5), B(10)	−10.8	6.7	H(5), H(10)	0.3	2.7
	B(7), B(8)	−22.9	−32.3	H(7), H(8)	−1.8	1.4
5H	B(7)	98.1	78.9[b]/79.9[c]	H(7)	10.6	7.5/7.5
	B(1), B(2), B(3), B(4)	28.3[a]	28.9/26.9	H(1), H(2), H(3), H(4)	7.5	5.0/5.0
	B(5), B(6)	−7.2	−15.4/−15.4	H(5), H(6)	0.7	1.2/1.2
				H_{BHB}	0.1	−1.3/−1.4
				H_{ReHB}	−10.8	−4.8/−6.8
6H	B(1), B(5)	88.3	72.8/79.0	H_{ReHB}	−9.3	−7.4/−7.3
	B(2), B(4)	48.3	45.0/41.9			
	B(3)	28.1	26.5/12.6			
7H	B(1), B(2)	87.3	78.0	H(3), H(6)	7.7	6.1
	B(3), B(6)	67.9	58.2	H(4), H(5)	6.4	5.3
	B(4), B(5)	59.3	47.5			
8H	B(7)	na[d]	87.4	H(7)	na	6.9
	B(1)		77.3	H(1)		
	B(6)		70.5	H(6)		6.1
	B(3), B(4)		71.0	H(3), H(4)		6.9
	B(2)		2.5	H(2)		2.7
	B(5)		−3.3	H(5)		1.7

[a] Fluxional behavior. [b] Isomer *a*. [c] Isomer *b*. [d] Nonavailable.

computed shifts.[69] Despite these caveats, the chemical shift calculations provide a stringent test of the validity of the calculated electronic structures of these rhenaboranes.

The ^{11}B and ^{1}H chemical shifts calculated for the series of rhenaboranes **1H**−**8H** are poor quantitatively relative to those calculated for boranes or carboranes. However, because the chemical shift range exhibited by the rhenaboranes is large, the calculations are of sufficient accuracy to make assignments for **1**−**4** that are consistent with the empirical ones based simply on boron connectivity and environment (see above). In general, the ^{11}B calculated values are systematically low (from 2 to 20 ppm), but experimental trends are correctly predicted and the ^{1}H chemical shifts are reproduced as well (Table 4). Noteworthy is the fact that ^{11}B chemical shifts computed for the five-connect boron atoms B(5), B(6) and the four-connect boron atoms B(4), B(7) in compound **2** strongly differ (14.5 and 106.7 ppm, respectively). Obviously, the resonance at 65.8 ppm for these four boron atoms is not due to an accidental overlap of two signals but rather to a low-barrier fluxional process of the framework boron atoms. Indeed, calculations using the Gaussian program package on a diamond−square−diamond rearrangement exchanging boron atoms reveal a barrier of only 5.5 kcal/mol at the B3LYP/LANL2DZ level of theory.

Consider **7**, for example, where the experimental ^{11}B NMR spectrum exhibits three different types of boron resonances with the two at higher field coupled to terminal hydrogen atoms. The empirical assignment was 87.3 ppm, B(1,2), and 67.9 and 59.3 ppm, B(3,6) and B(4,5), respectively (see above). The DFT calculations on **7H** yield values of 78.0, 58.2, and 47.5 ppm for B(1,2), B(3,6), and B(4,5). Hence, despite deviations of about 10−12 ppm, the trend is reproduced. Further, the computed ^{11}B chemical shifts of **4H** reproduce the large range of shifts measured experimentally for **4**. Empirical assignment of resonances at 60 and 50 ppm to the four-connect vertexes B(6,9) and B(2,3) and upfield resonances at 16, −11, and −23 ppm to the five-connect vertexes B(1,4), B(5,10), and B(7,8) are supported by the DFT computations. Pleasingly, the computations allow one to distinguish not only the difference in vertex connectivity (4 vs 5) but also the different B/Re environment of every boron atom.

As discussed above, more than one isomer is possible for compounds **5** and **6**, and the ^{11}B and ^{1}H chemical shifts were computed for the model isomer complexes **5aH** and **5bH** and **6aH** and **6bH**. The calculated values for both pairs compare well with the experimental data and do not allow differentiation (Table 4). Clearly conformations *a* and *b* for these compounds must rapidly interconvert in solution.

Electronic Requirements for Noncanonical Shapes. The satisfactory agreement of the calculated properties of these novel rhenaboranes with those observed shows that the theoretical approach provides a valid description of the electronic structure. Hence, these results should contain an explanation of the unusual structural behavior already described above. The language in which the explanation is developed is that of molecular orbitals, and the approach is fragment analysis which focuses attention on a small set of crucial orbital interactions.[70] Note that the

(69) Koch, W.; Holthauser, M. C. *A Chemist's Guide to Density Functional Theory*; Wiley-VCH: Weinheim, Germany, 2000.

(70) Hoffmann, R. *Science* **1981**, *211*, 995.

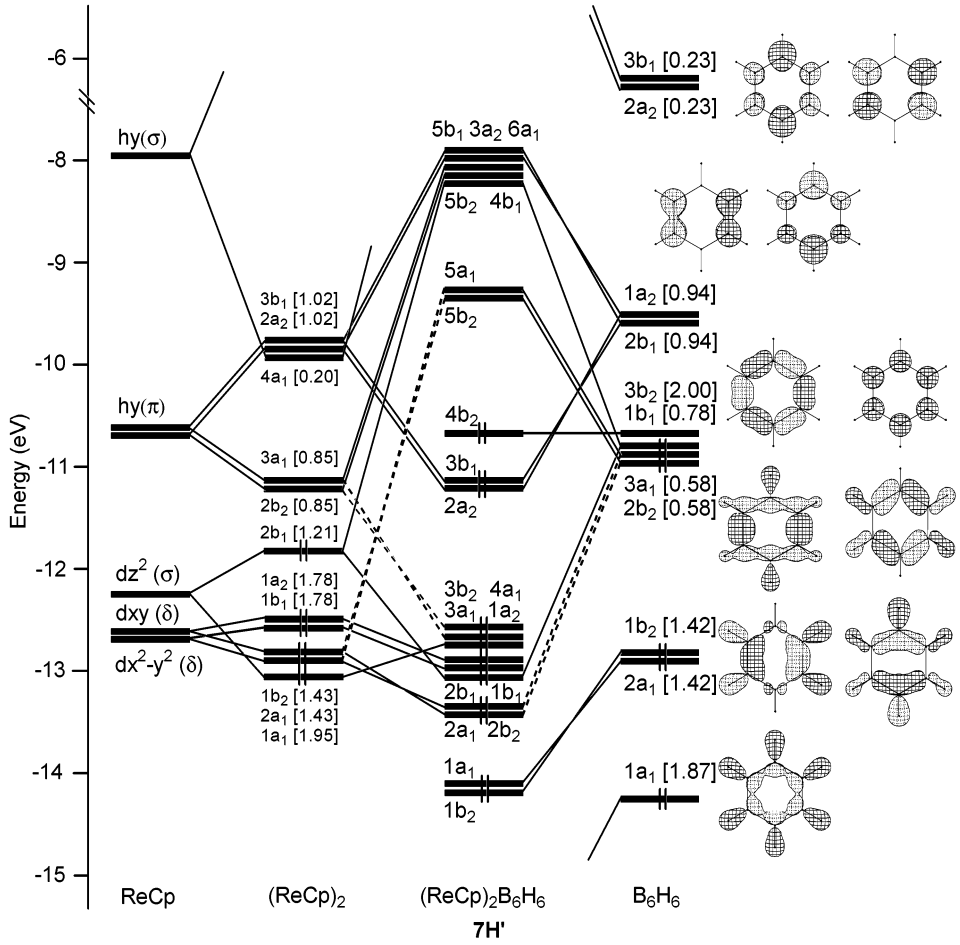

Figure 10. EH orbital interaction diagram for the model complex $(CpRe)_2B_6H_6$ (**7H′**) of C_{2v} symmetry. FMO occupations after interaction are given in brackets.

rhenaboranes studied all display qualitatively similar defects in structures and electron counts relative to the deltahedral structures and the Wade−Mingos rules, i.e., the same total vertex connectivity and (formally) p − 2 sep instead of p + 1 sep. This suggests a common origin in the nature of the interaction of the dirhenium fragment with the borane fragment.

A key compound is **7**, which can be considered either as a cluster or a triple-decker sandwich complex. Rhenaboranes **1**−**4** are clearly clusters but also can be considered as triple-decker sandwich complexes with increasingly complicated central "rings".[41,42] The latter viewpoint suggests partitioning into the Cp*Re···ReCp* fragment and the borane. This type of cap−ring model has a long history and provides one approach to counting electrons in organometallic and axial cluster systems.[71−73] With 24 valence electrons, molecule **7** is an electron-poor triple-decker sandwich dimetal complex. Other triple-decker complexes known are more electron-rich, with electron counts varying from 26 to 34 valence electrons.[74] The relationship between the stability of the metal−ring combination and the electron count is well understood for most of them.[58,75−77]

The 24-valence-electron triple-decker compound **7** provides a good introduction to the nature of the cap−ring interaction in these species. The EHMO diagram of $(CpRe)_2B_6H_6$ (**7H′**) obtained from the interaction of the frontier MOs of the bis(CpRe) fragment with the FMOs of the B_6H_6 hexagonal ring is shown in Figure 10. The FMOs of one CpRe unit are typical of any d^6 ML_3 organometallic fragment with one σ-type and two π-type hybrid FMOs lying above a set of three d orbitals (far left side of Figure 10). In the next column to the right, the interaction of the two CpRe entities in the absence of the central boron ring is shown. A Re−Re distance comparable to a Re−Re single bond generates significant level splittings particularly for the vacant σ-type hybrid FMOs. For 24 valence electrons (12 in the d orbital set) the bonding hybrid MOs are empty and all the bonding and antibonding d-type MOs are filled. Hence, only poor Re−Re bonding is expected at this stage.

Moving to the far right of Figure 10, some of the 30 MOs of a planar B_6H_6 fragment are shown and will be recognized as those of hypothetical $[C_6H_6]^{6+}$. The pertinent orbitals shown are five of the six π-type orbitals (three bonding orbitals, $1b_1$, $2b_1$, and $1a_2$, and two antibonding orbitals, $3b_1$ and $2a_2$). In addition, six σ-type orbitals lie in the same energy region. Numerous, strong interactions occur between the FMOs of the metal and borane fragments. The two empty π-type orbitals of the borane fragment, $1a_2$ and $2b_1$, interact strongly with the two

(71) Hoffmann, R.; Lipscomb, W. N. *J. Chem. Phys.* **1962**, *36*, 2179.
(72) Jemmis, E. D. *J. Am. Chem. Soc.* **1982**, *104*, 7017.
(73) Jemmis, E. D.; Schleyer, P. v. R. *J. Am. Chem. Soc.* **1982**, *104*, 4781.
(74) Lauher, J. W.; Elian, M.; Summerville, R. H.; Hoffmann, R. *J. Am. Chem. Soc.* **1976**, *98*, 3219.
(75) Reddy, A. C.; Jemmis, E. D.; Scherer, O. J.; Winter, R.; Heckmann, G.; Wolmershäuser, G. *Organometallics* **1992**, *11*, 3894.
(76) Tremel, W.; Hoffmann, R.; Kertesz, M. *J. Am. Chem. Soc.* **1989**, *111*, 2030.
(77) Grimes, R. N. *Coord. Chem. Rev.* **1979**, *28*, 47.

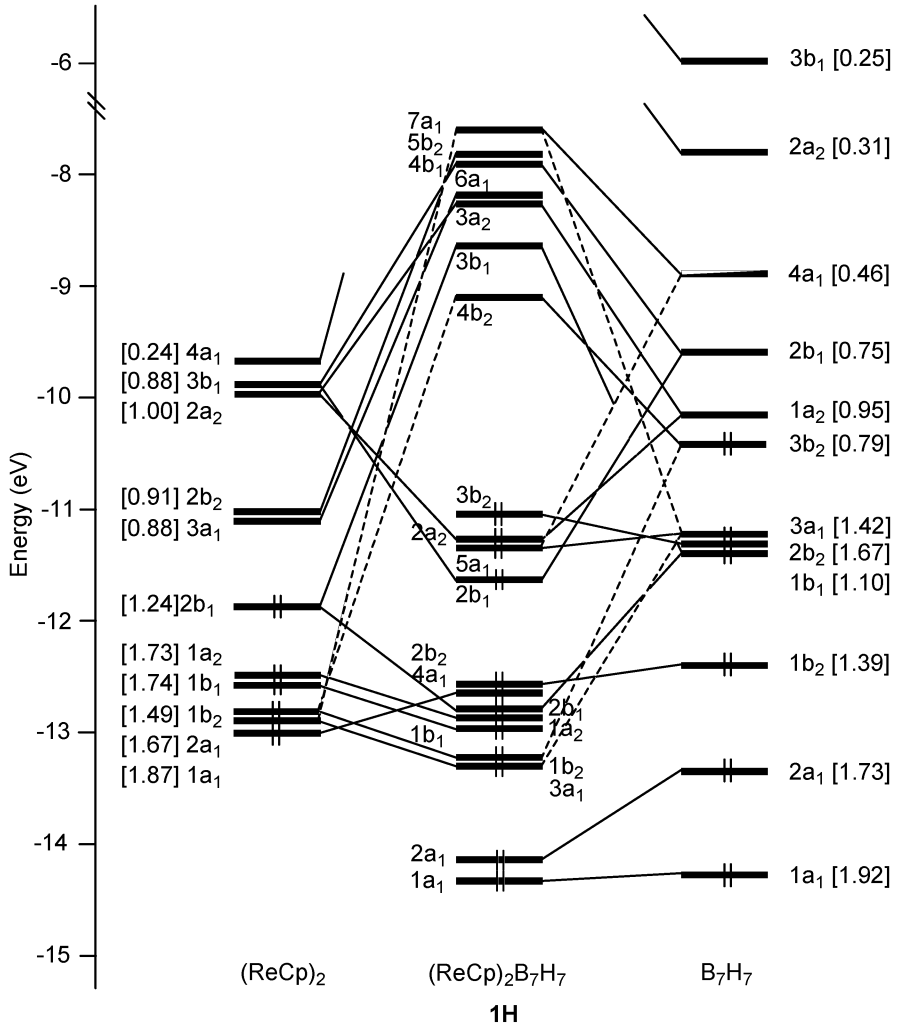

Figure 11. EH orbital interaction diagram for the model complex $(CpRe)_2B_7H_7$ (**1H**) of C_{2v} symmetry. FMO occupations after interaction are given in brackets.

empty π^* metallic orbitals ($2a_2$ and $3b_1$), leading to stabilized bonding Re−B MOs ($2a_2$ and $3b_1$) and destabilized Re−B antibonding MOs ($3a_2$ and $5b_1$). The other borane π-type bonding FMO $1b_1$ interacts strongly with the Re−Re d_{z^2} σ^* antibonding FMO $2b_1$. The borane one is destabilized ($4b_1$), whereas the metallic one is stabilized ($1b_1$). Some interaction between the high-lying borane π^* FMOs and corresponding MOs of the bis-Re fragment is revealed by electron occupation after interaction (Figure 10). In addition, strong interactions occur between the two borane π-type FMOs ($2b_2$ and $3a_1$) and the two Re−Re bonding π-type FMOs ($1b_2$ and $2a_1$). In all cases the Re−B bonding combinations are strongly stabilized ($2b_2$ and $2a_1$), and the antibonding combinations are destabilized ($5b_2$ and $5a_1$).

As shown in the middle of Figure 10, the 24 valence electrons of **7H′** fill the bonding combinations and leave the antibonding combinations empty, thereby generating the large HOMO ($4b_2$)−LUMO ($5b_2$) gap already noted from the DFT calculations. Is there any cross-cluster Re−Re bond in this species? Electron occupation of all the metal FMOs after interaction with the borane ring, some of which are Re−Re bonding and others Re−Re antibonding, suggests weak Re−Re bonding if any. However, the filled Re−Re d_{z^2} σ^* antibonding FMO $2b_1$ in the CpRe···ReCp fragment is partially emptied in the strong interaction with the borane ring. This would support the presence of weak cross-cluster bonding.

Is it now possible to merge the triple-decker and cluster views of **7** and thereby extend the analysis to **1**−**4**? Let us first consider the electronic demands of the borane entity. A glance at the FMOs of the B_6H_6 ring indicates that six electrons are missing to fill all its bonding−nonbonding MOs (Figure 10). This borane ring can be defined as an *arachno* cluster with two unoccupied apexes. Filling the three bonding−nonbonding MOs $3b_2$, $2b_1$, and $1a_2$ would yield the expected count of 9 sep for such an arrangement, analogous to that of C_6H_6. Interaction of these vacant orbitals with occupied FMOs of the bis-Re fragment allows the formal transfer of six metal electrons to metal−boron bonding MOs to satisfy the 9 sep electronic requirement of the borane ring. These six metal electrons must come from the "t_{2g}" set and are no longer nonbonding but rather Re−B bonding. Therefore, they can be included in the number of sep.

Can this approach be used for the larger systems? An analysis of the interaction MO diagram of the next higher member of the series, $(CpRe)_2B_7H_7$ (**1H**), indicates that we can do so (Figure 11). Consider the B_7 borane "torus" spanning the CpRe entities in **1H**, an *arachno* cluster with two metal caps. Its FMOs shown on the right of the figure can be derived from those of the B_6H_6 ring by substitution of a BH unit by a B_2H_2 fragment

Chart 6. Green Vertices Label Those Lost in the *debor* Operation

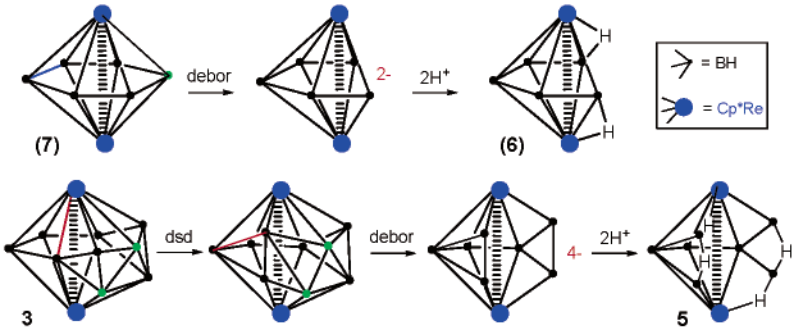

perpendicularly to the plane containing the other five boron atoms. This increases the number of orbitals by five. Nevertheless, this substitution does not strongly modify the bonding properties of the borane FMOs. Mainly due to a lowering of symmetry, there is a greater distribution in energy with a substantial energy gap between FMOs $4a_1$ and $2a_2$ (Figure 11), but the interactions with the FMOs of the metallic fragment are comparable to those in **7H′**. This is reflected in the similar group electron occupation of the metallic orbitals after interaction (13.65, **7H′** vs 12.67 electrons, **1H**) and the total Re−Re overlap populations (0.01, **7H′** and 0.03, **1H)**. As found for **7H′**, the bonding in **1H** is mainly governed by interactions occurring between the bonding π-type orbitals of the borane fragment and the metallic orbitals $2b_1$ (σ*), $1a_2$ and $1b_1$ (δ*), and $2a_2$ and $3b_1$ (π*). The π-type back-donation from occupied metallic orbitals into the high-lying acceptor π*-type borane orbitals $3b_1$ and $2a_2$ is slightly larger than in **7H** (electron occupation of 0.25 and 0.31 vs 0.23 and 0.23 for the corresponding B_6H_6 orbitals). The Re−Re σ* antibonding d_{z^2}-type metallic orbital $2b_1$ interacts strongly with the occupied π-type orbital $1b_1$ of the borane fragment. As in **7H′**, the antibonding combination is destabilized and becomes vacant ($3b_1$). Moreover, the occupied δ-type metallic orbitals $1b_2$ and $2a_1$ interact with the σ-type borane orbitals $3b_2$ and $3a_1$. These destabilizing interactions are less important than in **7H′** but still significant.

Importantly, the addition of six extra electrons fills all the bonding and nonbonding MOs and leads to a substantial HOMO−LUMO gap between the FMOs $4a_1$ and $2a_2$ for the B_7 unit, similarly to the hexagonal B_6H_6 ring (vide supra). The formally vacant bonding FMOs $1a_2$, $2b_1$, and $4a_1$ strongly mix with low-lying occupied metallic FMOs. Such interaction leads to an important electron transfer (formally 6 as in **7H′**) from the "t_{2g}" set of the metal fragments to these borane acceptor orbitals and creates a large HOMO−LUMO gap for the count of 10 sep (i.e., $n + 3$) expected for a bicapped B_7 *arachno* species.

A check shows that **2**−**4** obey the guidelines proposed for compounds **7H′** and **1H**. Thus, in an aufbau process, any member of the $(Cp^*Re)_2B_nH_n$ family can be generated from its predecessor by the addition of a two-electron BH fragment to the borane torus capped above and below by three-electron metal units. Hence the $n + 3$ guideline holds for the whole $(Cp^*Re)_2B_nH_n$ series, which can be reasonably depicted as clusters with 11, 12, and 13 sep, respectively: a cluster count that can only be realized in the oblate shapes adopted.

With this principle established, the structures of **5** and **6** can be easily rationalized. As shown in Chart 6, starting from **7** and **3** one can generate the observed structures of **5** and **6** using the *debor* process so useful in borane structural chemistry.[2,4,78] Thus, removing a BH vertex and replacing it with two electrons followed by protonation generates the structure of **5**. For **6**, a dsd rearrangement to give two six-coordinate Re vertexes followed by *debor* twice and protonation generates the observed structure. Clearly the number of possible structures to be generated from **1**−**4** rivals those of boranes related in the same fashion to the *closo*-$[B_nH_n]^{2-}$ anions.[78] The challenge is there for the synthetic chemist.

Discussion

The isolobal analogy emphasizes the similarities between transition metal fragments and main group fragments. Its success in explaining known chemistry as well as provoking new chemistry has led to a complaisant view that this is sufficient for understanding metallaboranes and related systems. In fact, to date, with the important exception of the body of work mentioned in the Introduction[22] coming largely from the Kennedy laboratory, it is. But the rhenaboranes described here show that the earlier transition metals produce sufficiently large structural perturbations that the role of the metal fragments can be more precisely described. The known "*isocloso*" aka "*hypercloso*" compounds are now seen to be incremental structural variants of the canonical geometries pointing toward the larger structural perturbation observed in the hypoelectronic rhenaboranes. These are, in retrospect, a logical development of the "disobedient skeletons" of Kennedy.[22] Some analogies illustrate the point.

Consider the organometallic dimer $[CpFe(CO)_2]_2$. The one-orbital, one-electron $CpFe(CO)_2$ fragment is isolobal with CH_3 and, hence, the metal dimer is isolobal with C_2H_6. The filled t_{2g} metal d set are effectively nonbonding. Moving to group 6 from 8 does not give a one-orbital $CpMo(CO)_2$ fragment isolobal with $[CH_3]^{2+}$ but rather one isolobal with the three-orbital, three-electron CH fragment: $[CpMo(CO)_2]_2$ is isolobal with HC≡CH. Hoffmann has referred to this as going "into the t_{2g} set" to emphasize that as the effective nuclear charge decreases, more of the nine metal valence orbitals of the metal can get involved in bonding.[70] Thus, there is no reason to rule out this possibility in metallaborane chemistry.

Further, metal fragments can engage in bonding modes not available to main group atoms. Pertinent to this discussion, two CH fragments generate a carbon−carbon triple bond, but two $[ReCl_4]^-$ fragments generate a quadruple bond: something not

(78) Rudolph, R. W. *Acc. Chem. Res.* **1976**, *9*, 446.

Chart 7

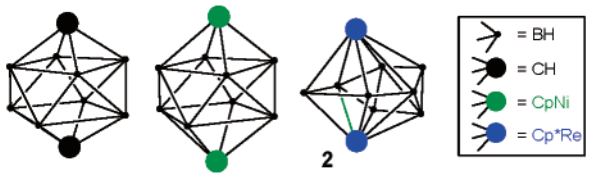

possible for the main group fragments.[79] A geometry of $[Re_2Cl_8]^{2-}$ with face to face, eclipsed square-planar $[ReCl_4]^-$ fragments is required to permit a δ symmetry bonding interaction; new bonding modes generate observable geometric consequences.

Now compare 1,10-$(HC)_2B_8H_8$, 1,10-$(CpNi)_2B_8H_8$,[19,80,81] and $(Cp^*Re)_2B_8H_8$ (Chart 7). We know that in each case the pair of axial heteroatom fragments contributes 3 sep to the cluster bonding network. The CH and CpNi fragments each use three FMOs, one of σ and two of π symmetry, and produce bicapped square antiprismatic geometries analogous to that of the canonical borane $[B_{10}H_{10}]^{2-}$. But, if the pair of Cp*Re fragments in **2** also contribute 3 sep to cluster bonding, why the noncanonical geometry? On the basis of the theoretical results discussed above, an interaction within the Cp*Re···ReCp* fragment is necessary to generate a set of FMOs that can form strong bonding and antibonding combinations with the available borane fragment orbitals. This is possible only if the borane fragment geometry is modified into the ring-like structures observed. Those adopted by the borane fragment both generate a matching set of FMOs *and* permit the necessary Re−Re interaction. Hence, noncanonical structures with increased numbers of Re−B interactions and decreased B−B interactions, but the same total vertex connectivities, are observed. Finally, $(Cp^*Re)_2B_{10}H_{10}$ appears to be the limiting stoichiometry simply because the addition of another BH fragment would force the Re atoms too far apart to permit the necessary cross-cluster interaction.

Just as the formation of a quadruple bond in $[Re_2Cl_8]^{2-}$ has observable geometric consequences, so too the utilization of the filled t_{2g} sets of the Cp*Re fragments requires the observed noncanonical structures of **1**−**8**. It is satisfying to learn that main group cluster structure can be driven by transition metal variation; the possibilities for new chemistry are substantial.

Experimental Section

General Procedures. All the operations were conducted under an Ar atmosphere using standard Schlenk techniques.[82] Solvents were distilled prior to use under N_2. BH_3·THF, $BHCl_2$·SMe_2, and $LiBH_4$ in THF (Aldrich) were used as received. $(Cp^*ReH_2)_2B_4H_4$ was prepared as described previously.[83] NMR spectra were recorded on a 300 or 500 MHz Varian or 400 MHz Bruker FT-NMR spectrometer. Residual solvent protons were used as reference (δ, ppm, benzene, 7.15), while a sealed tube containing $[Me_4N(B_3H_8)]$ in acetone-d_6 (δ_B, ppm, −29.7) was used as an external reference for the ^{11}B NMR. Infrared spectra were obtained on a Nicolet 205 FT-IR spectrometer. Mass spectra were obtained on JEOL JMS-AX505HA mass spectrometer with perfluoro kerosene as standard.

$(Cp^*Re)_2B_nH_n$ (n = 8−10, 2−4). To a 100 mL Schlenk tube, containing 0.15 g (0.21 mmol) of $(Cp^*ReH_2)_2B_4H_4$ in 15 mL of toluene, was added 8 equiv of BH_3·THF very slowly by syringe. Immediately after the addition of BH_3·THF the reaction mixture was heated for 26 h at 90 °C and then allowed to cool to room temperature. Volatiles were removed in vacuo, and the residue was extracted in hexane/CH_2Cl_2 (9:1 v/v) and filtered through Celite. After removal of solvent from the filtrate, the residue was subjected to chromatographic workup using silica gel TLC plates. Elution with a hexane/CH_2Cl_2 (8:2 v/v) mixture yielded four very closely spaced bands. The first, yellow band to elute was characterized spectroscopically as **1** (0.02 g, 17%), the second, orange-red band as **2** (0.05 g, 38%), the third, red band as **3** (0.01 g, 10%), and the fourth, yellow band as **4** (0.01 g, 7%). X-ray quality crystals were grown by slow diffusion of the CH_2Cl_2/hexane (9:1 v/v) solution of $(Cp^*Re)_2B_nH_n$ (n = 7−10) at 5 °C.

Compound 2. MS (EI), P+ (max) = 736 (isotopic pattern for 2Re and 8B atoms). Calculated mass for $^{12}C_{20}{}^1H_{38}{}^{11}B_8{}^{187}Re_2$, 739.2755, obsd, 739.2722 (exact mass measurement done on M − 1). ^{11}B NMR (C_6D_6, 22 °C): δ 97.92 (d, J_{B-H} = 163 Hz, 2B), 65.76 (d, J_{B-H} = 136 Hz, 4B), 21.92 (d, J_{B-H} = 141 Hz, 2B). ^{1}H NMR (C_6D_6, 22 °C): δ 9.86 [pcq, 2BH*t*], 9.02 [pcq, 4BH*t*], 0.32 [pcq, 2BH*t*], 1.86 (s, 30H, 2Cp*). IR (KBr, cm^{-1}): 2521 w, 2443 w (B−H*t*, in CH_2Cl_2).

Compound 3. MS (EI), P+ (max) = 748 (isotopic pattern for 2Re and 9B atoms). Calculated mass for $^{12}C_{10}{}^1H_{39}{}^{11}B_9{}^{187}Re_2$, 751.2926, obsd, 751.2908 (exact mass measurement done on M − 1). ^{11}B NMR (C_6D_6, 22 °C): δ 94.08 (d, J_{B-H} = 168 Hz, 2B), 76.19 (d, J_{B-H} = 153 Hz, 2B), 35.49 (d, J_{B-H} = 129 Hz, 2B), 1.09 (d, J_{B-H} = 130 Hz, 2B), −28.73 (d, J_{B-H} = 130 Hz, 1B). ^{1}H NMR (C_6D_6, 22 °C): δ 11.21 [pcq, 2BH*t*], 10.23 [pcq, 2BH*t*], 8.46 [pcq, 2BH*t*], −0.12 [pcq, 2BH*t*], −2.26 [pcq, 1BH*t*], 1.92 (s, 15H, 1Cp*), 1.51 (s, 15H, 1Cp*). IR (KBr, cm^{-1}): 2532 w, 2430 w (B−Ht, in CH_2Cl_2).

Compound 4. MS (EI), P+ (max) = 760 (isotopic pattern for 2Re and 10B atoms). Calculated mass for $^{12}C_{10}{}^1H_{40}{}^{11}B_{10}{}^{187}Re_2$, 763.3098, obsd, 763.3126 (exact mass measurement done on M − 1). ^{11}B NMR (C_6D_6, 22 °C): δ 59.95 (d, J_{B-H} = 175 Hz, 2B), 50.39 (d, J_{B-H} = 158 Hz, 2B), 16.14 (d, J_{B-H} = 135 Hz, 2B), −10.77 (d, J_{B-H} = 144 Hz, 2B), −22.91 (d, J_{B-H} = 132 Hz, 2B). ^{1}H NMR (C_6D_6, 22 °C): δ 8.56 [pcq, 2BH*t*], 6.84 [pcq, 2BH*t*], 5.96 [pcq, 2BH*t*], 0.28 [pcq, 2BH*t*], −1.75 [pcq, 2BH*t*], 1.43 (s, 30H, 2Cp*). IR (KBr, cm^{-1}): 2531 w, 2451 w (B−Ht) (in CH_2Cl_2).

$(Cp^*ReH)_2B_7H_9$ (5). To a 100 mL Schlenk tube, containing 0.15 g (0.21 mmol) of $(Cp^*ReH_2)_2B_4H_4$ in 15 mL of toluene, was added 3 equiv of BH_3·THF very slowly by syringe. The reaction mixture was immediately heated for 15 h at 75 °C. Volatiles were removed in vacuo, and the residue was extracted in hexane and filtered through Celite. After removal of solvent from the filtrate, the residue was subjected to chromatographic workup using silica gel TLC plates. Elution with hexane yielded four very closely spaced bands. The first, yellow band to elute was characterized spectroscopically as **5** (0.026 g, 17%), the second, yellow band as **1** (0.048 g, 32%), the third, orange red band as **2** (0.018 g, 12%), and the fourth, red band as **3** (0.006 g, 4%). X-ray quality crystals were grown by slow diffusion of the CH_2Cl_2/hexane (9:1 v/v) solution of **5** at 5 °C.

Compound 5. MS (EI), P+ (max) = 726 (isotopic pattern for 2Re and 7B atoms). Calculated mass for $^{12}C_{20}{}^1H_{41}{}^{11}B_7{}^{187}Re_2$, 732.2982, obsd, 732.2948. ^{11}B NMR (C_6D_6, 22 °C): δ 98.1 (d, J_{B-H} = 162 Hz, 1B), 28.3 (d, J_{B-H} = 130 Hz, 4B), −7.2 (d, J_{B-H} = 141 Hz, 2B). ^{1}H NMR (C_6D_6, 22 °C): δ 10.61 [pcq, 1BH*t*], 7.51 [pcq, 4BH*t*], 0.72 [pcq, 2BH*t*], 0.04 [br, 2B−H−B], 1.76 (s, 30H, 2Cp*), −10.77 [s, 2Re−H−B]. IR (KBr, cm^{-1}): 2498 w, 2444 w (B−H*t*, in hexane).

$(Cp^*ReH)_2B_5Cl_5$ (6), $(Cp^*Re)_2B_6H_4Cl_2$ (7), and $(Cp^*Re)_2B_7H_6Cl$ (8). In a typical reaction, $(Cp^*ReH_2)_2B_4H_4$ (0.05 g, 0.07 mmol) was loaded in a 100 mL Schlenk flask with 10 mL of freshly distilled toluene. To this reaction mixture was added a 4-fold excess of $BHCl_2$·

(79) Cotton, F. A.; Walton, R. A. *Multiple Bonds Between Metal Atoms*; Wiley: New York, 1983.
(80) Sullivan, B. P.; Leyden, R. N.; Hawthorne, M. F. *J. Am. Chem. Soc.* **1975**, *97*, 456.
(81) Leyden, R. N.; Sullivan, B. P.; Baker, R. T.; Hawthorne, M. F. *J. Am. Chem. Soc.* **1978**, *100*, 3758.
(82) Shriver, D. F.; Drezdzon, M. A. *The Manipulation of Air-Sensitive Compounds*, 2nd ed.; Wiley-Interscience: New York, 1986.
(83) Ghosh, S.; Shang, M.; Fehlner, T. P. *J. Organomet. Chem.* **2000**, *614*−*15*, 92.

SMe_2, and the reaction mixture was stirred for 10 min at room temperature, during which time the orange-yellow color of the starting material changed to deep red accompanied with the evolution of gas. The ^{11}B NMR spectrum of this reaction mixture shows four resonances, none of which are due to the starting material. The resultant reaction mixture was then thermolyzed at 75 °C for 20 h. Volatiles were removed in vacuo (under a warm water bath for 6 h), and the residue was extracted in toluene and quickly filtered through Celite mixed with a very small amount of silica gel. After removal of solvent from the filtrate, the residue was redissolved in a small amount of CH_2Cl_2/hexane (2:8 v/v) and kept in a freezer for crystallization. Brown crystals (not X-ray quality) of **6** (0.03 g, 52%) precipitated overnight. The supernatant solution was chromatographed using silica gel TLC plates. Elution with a hexane/CH_2Cl_2 (7:3 v/v) mixture yielded five bands, out of which four are very closely spaced. The first band (purple-brown) was an unknown compound or compounds, the second band (orange-yellow) was **7** (0.002 g, 4%), the third band (yellow) was a mixture of two compounds, **1** and an unknown metallaborane, and the fourth band (orange-yellow) was **8** mixed with **1**. X-ray quality crystals of **6**−**8** were grown by slow diffusion, CH_2Cl_2/hexane (9:1 v/v), at 5 °C.

Compound 6. MS (EI), P+ (max) = 874 (isotopic pattern for 2Re, 5B, and 5Cl atoms). ^{11}B NMR (C_6D_6, 22 °C): δ 88.3 (s, 2B), 48.3 (s, 2B), 28.1 (s, 1B). ^1H NMR (C_6D_6, 22 °C): δ −9.34 [s, 2Re−H], 1.80 (s, 30H, 2Cp*).

Compound 7. MS (EI), P+ (max) = 782 (isotopic pattern for 2Re, 6B, and 2Cl atoms). ^{11}B NMR (C_6D_6, 22 °C): δ 87.3 (s, 2B), 67.9 (d, J_{B-H} = 158 Hz, 2B), 59.3 (d, J_{B-H} = 161 Hz, 2B). ^1H NMR (C_6D_6, 22 °C): δ 7.7 [pcq, 2BH*t*], 6.4 [pcq, 2BH*t*], 1.96 (s, 30H, Cp*).

X-ray Structure Determinations. Data for **2**−**5** have been deposited previously with the Cambridge Crystallographic Data Centre (CCDC 151686, 151687, 151688, 155582). Copies of the data can be obtained free of charge on application to CCDC, 12 Union Road, Cambridge CB21EZ, UK (fax: (+44)1223-336-033; e-mail: deposit@ccdc.cam.ac.uk). The CIF file for **7** was also deposited previously,[41] and this material is available free of charge via the Internet at http://pubs.acs.org.

$(Cp^*Re)_2B_8H_8$ (2). An orange needle-like crystal of **2** was mounted on a glass fiber for examination on an Enraf-Nonius CAD 4 diffractometer. Most of the non-hydrogen atoms were located by the direct method; the remaining non-hydrogen atoms were found in succeeding difference Fourier syntheses. After all non-hydrogen atoms were refined anisotropically, difference Fourier synthesis located most of the hydrogen atoms. In the final refinement hydrogen atoms were refined isotropically with idealized riding models. Formula, $C_{20}H_{38}B_8Re_2$; fw, 737.38; crystal system, tetragonal; space group, $P4_2bc$; dimensions, 0.45 × 0.10 × 0.10 mm; unit cell, a = 23.5699(15) Å, c = 9.4344(8) Å; T, 293(2) K; Z, 8; GOF, 0.980; R1 = 0.0517, wR2 = 0.0656. CCDC-151686.

$(Cp^*Re)_2B_9H_9$ (3). An orange needle-like crystal of **3** was mounted on a glass fiber for examination on a Bruker Smart CCD diffractometer. Most of the non-hydrogen atoms were located by the direct method; the remaining non-hydrogen atoms were found in succeeding difference Fourier syntheses. After all non-hydrogen atoms were refined anisotropically, difference Fourier synthesis located most of the hydrogen atoms. In the final refinement hydrogen atoms were refined isotropically with idealized riding models. The polarity of the structure was determined by a practical zero value of the Flack absolute structure parameter −0.020(14), although both enantiomers coexisted. Formula, $C_{20}H_{39}B_9Re_2$; fw, 749.20; crystal system, tetragonal; space group, $P4_2bc$; dimensions, 0.51 × 0.10 × 0.10 mm; unit cell, a = 23.7534(10) Å, c = 9.2871(15) Å; T, 294(2) K; Z, 8; GOF, 0.820; R1 = 0.0885, wR2 = 0.0460. CCDC-151687.

$(Cp^*Re)_2B_{10}H_{10}$ (4). A yellow needle-like crystal of **4** was mounted on a glass fiber for analysis on a Bruker Smart CCD diffractometer. Most of the non-hydrogen atoms were located by the direct method; the remaining non-hydrogen atoms were found in succeeding difference Fourier syntheses. After all non-hydrogen atoms were refined anisotropically, difference Fourier synthesis located most of the hydrogen atoms. In the final refinement hydrogen atoms were refined isotropically with idealized riding models. The polarity of the structure was determined by a practical zero value of the Flack absolute structure parameter 0.00(2), although both enantiomers coexisted. Formula, $C_{20}H_{40}B_{10}Re_2$; fw, 761.02; crystal system, tetragonal; space group, $P4_2bc$; dimensions, 0.45 × 0.10 × 0.10 mm; unit cell, a = 23.365(3) Å, c = 9.7768(15) Å; T, 294(2) K; Z, 8; GOF, 0.804; R1 = 0.1006, wR2 = 0.0746. CCDC-151688.

$(Cp^*Re)_2B_7H_{11}$ (5). A yellow crystal of **5** was mounted for analysis on a Bruker Smart CCD diffractometer. All non-hydrogen atoms were refined anisotropically. All Cp* hydrogen atoms were placed in idealized locations; the seven terminal B−H hydrogen atoms were located and refined. The four bridging hydrogen atoms were not located. Formula, $C_{20}H_{41}B_7Re_2$; fw, 729.60; crystal system, triclinic; space group, $P\bar{1}$; dimensions, 0.40 × 0.0.30 × 0.20 mm; unit cell, a = 8.7967(2) Å, b = 17.7865(3) Å, c = 18.0509(4) Å, α = 111.5640(10)°, β = 102.924(2)°, γ = 99.4110(10)°; T, 173(2) K; Z, 8; GOF, 1.015; $R(F)$ = 4.85%, $R(wF^2)$ = 13.72%. CCDC 155582.

$(Cp^*ReH)_2B_5Cl_5$ (6). A crystal of **6** was placed in inert oil, mounted on a glass pin, and transferred to the cold gas stream of the diffractometer. Crystal data were collected and integrated using a Bruker Apex system, with graphite-monochromated Mo Kα (λ = 0.71073 Å) radiation at 170 K. The structure was solved by heavy atom methods using SHELXS-97 and refined using SHELXL-97 (Sheldrick, G. M., University of Göttingen). Non-hydrogen atoms were found by successive full matrix least squares refinement on F^2 and refined with anisotropic thermal parameters. Hydrogen atoms were placed at idealized positions, and a riding model with fixed thermal parameters [u_{ij} = 1.2U_{ij}(eq) for the atom to which they are bonded] was used for subsequent refinements. Formula, $C_{20}H_{30}B_5Cl_5Re_2$; fw, 874.14; crystal system, monoclinic; space group, $P2(1)/n$; dimensions, 0.49 × 0.37 × 0.29 mm; unit cell, a = 9.7529(5) Å, b = 14.7661(7) Å, c = 18.5310(9) Å, β = 90.4320(10)°; T, 170(2) K; Z, 4; GOF, 1.095; R1 = 0.0365, wR2 = 0.0902.

$(Cp^*Re)_2B_6H_4Cl_2$ (7). A crystal of **7** was placed in inert oil, mounted on a glass pin, and transferred to the cold gas stream of the diffractometer. Crystal data were collected and integrated using a Bruker Apex system, with graphite-monochromated Mo Kα (λ = 0.71073 Å) radiation at 170 K. The structure was solved by heavy atom methods using SHELXS-97 and refined using SHELXL-97 (Sheldrick, G. M., University of Göttingen). Non-hydrogen atoms were found by successive full matrix least squares refinement on F^2 and refined with anisotropic thermal parameters. Hydrogen atoms were placed at idealized positions, and a riding model with fixed thermal parameters [u_{ij} = 1.2U_{ij}(eq) for the atom to which they are bonded] was used for subsequent refinements. Although the unit cell refined as nearly monoclinic, systematic absences were not consistent with monoclinic space groups. Therefore, the space group was determined to be $P\bar{1}$ with pseudomerohedral twinning (matrix applied: −1 0 0 0−1 0 0 0 1), resulting in two molecules per asymmetric unit. The two components of the twin were determined to be present in a 76%:24% ratio. Formula, $C_{20}H_{34}B_6Cl_2Re_2$; fw, 782.63; crystal system, triclinic; space group, $P\bar{1}$; dimensions, 0.30 × 0.30 × 0.20 mm; unit cell, a = 10.5106(10) Å, b = 14.3786(13) Å, c = 16.7764(16) Å, α = 89.965(2)°, β = 89.905(2)°, γ = 85.253(2)°; T, 170(2) K; Z, 4; GOF, 1.076; R1 = 0.0421, wR2 = 0.0872.

$(Cp^*Re)_2B_7H_6Cl$ (8). A crystal of **8** was placed in inert oil, mounted on a glass pin, and transferred to the cold gas stream of the diffractometer. Crystal data were collected and integrated using a Bruker Apex system, with graphite-monochromated Mo Kα (λ = 0.71073 Å) radiation at 170 K. The structure was solved by direct methods using SHELXS-97 and refined using SHELXL-97 (Sheldrick, G. M., University of Göttingen). Non-hydrogen atoms were found by successive full matrix least squares refinement on F^2 and refined with anisotropic thermal parameters, except for the disordered Cp* ring, the

components of which were isotropically refined. Hydrogen atoms were placed at idealized positions, and a riding model with fixed thermal parameters [$u_{ij} = 1.2U_{ij}$(eq) for the atom to which they are bonded] was used for subsequent refinements. One hydride atom was not included in the refinement, as the chloride was disordered (located on B1 80% of the time and B6 20% of the time), and the corresponding hydride atom (located on B1 20% of the time and B6 80% of the time) was not included. While one Cp* ring was ordered, the other had a rotational disorder, with two different locations for the rings in a 50:50 ratio. Formula, $C_{20}H_{36}B_7ClRe_2$; fw, 760.01; crystal system, monoclinic; space group, $P2(1)/c$; dimensions, $0.26 \times 0.23 \times 0.07$ mm; unit cell, $a = 9.3182(5)$ Å, $b = 11.6312(7)$ Å, $c = 23.1331(13)$ Å, $\beta = 93.0820(10)°$; T, 170(2) K; Z, 4; GOF, 1.064; R1 = 0.0430, wR2 = 0.0972.

Theoretical Calculations. Extended Hückel calculations were carried out on the DFT-optimized geometries of the models **1H**−**8H** within the extended Hückel formalism[84] using the CACAO program.[85] The Slater exponents (ζ) and the valence shell ionization potentials (H_{ii} in eV) were respectively the following: 1.3, −13.6 for H 1s; 1.3, −15.2 for B 2s; 1.3, −8.5 for B 2p; 1.625, −21.4 for C 2s; 1.625, −11.4 for C 2p; 2.183, −26.3 for Cl 3s; 1.733, −14.2 for Cl 3p; 2.398, −9.36 for Re 6s; 2.372, −5.96 for Re 6p. The H_{ii} value for Re 5d was set equal to −12.66. A linear combination of two Slater-type orbitals with exponents $\zeta_1 = 5.343$ and $\zeta_2 = 2.277$ with the weighting coefficients $c_1 = 0.6662$ and $c_2 = 0.5910$ was used to represent the Re 5d atomic orbitals.

Density functional theory calculations were carried out on the model complexes **1H**−**8H** using the Amsterdam Density Functional (ADF) program[86] developed by Baerends and co-workers.[87−90] The Vosko−Wilk−Nusair parametrization[91] was used for the local density approximation (LDA) with gradient corrections for exchange (Becke88)[92,93] and correlation (Perdew86).[94] The geometry optimization procedure was based on the method developed by Versluis and Ziegler.[95] Relativistic corrections were added using the ZORA (zeroth order regular approximation) scalar Hamiltonian.[96−98] The electronic configurations of the molecular systems were described by a triple-ζ Slater-type orbital (STO) basis set for H 1s, C 2s and 2p, B 2s and 2p, and Cl 3s and 3p augmented with a 3d single-ζ polarization function for C, B, and Cl and with a 2p single-ζ polarization function for H. A double-ζ STO basis set was used for Re 5s and a triple-ζ STO basis set was used for Re 4f, 5p, 5d augmented with a single-ζ 6p. A frozen-core approximation was used to treat the core electrons of B, Cl, C, H, and Re.

The adiabatic ionization potential computed for the models $(CpRe)_2B_nH_n$ (**1H**−**4H**) was defined as the energy difference between optimized geometries of the monocationic and the neutral species. The vertical ionization potential computed for all the models corresponds to the removal of one electron from the fixed geometry of the neutral molecule.

Calculations of the NMR shielding tensors employed gauge-including atomic orbitals (GIAOs),[99−102] using the implementation of Schreckenbach, Wolff, Ziegler, and co-workers.[103−107] TMS ($SiMe_4$) was used as internal standard for the ^{1}H NMR chemical shift calculations. B_2H_6 was used as a primary reference for the ^{11}B chemical shift calculations ($\delta(B_2H_6) = 16.6$ ppm was used for conversion to the standard experimental $BF_3{\cdot}OEt_2$ scale). The studies of the fluxional behavior of compound **2** were carried out using the Gaussian package at the B3LYP/LANL2DZ level of theory.[108]

Acknowledgment. The support of the National Science Foundation (NSF CHE 99-86880) is gratefully acknowledged. These studies were also facilitated by travel grants from the National Science Foundation (INT 02-31792, USA) and the Centre National de la Recherche Scientifique (CNRS 03N92/0123, France). The group of Rennes thanks the Pôle de Calcul Intentif de l'Ouest (PCIO) of the University of Rennes for computing facilities.

Supporting Information Available: CIF files for **6** and **8** (there are alerts in the CIF of **8**) and table of energies and compositions of selected orbitals in the HOMO/LUMO region of **1H**−**8H**. This material is available free of charge via the Internet at http://pubs.acs.org.

JA039770B

(84) Hoffmann, R. *J. Chem. Phys.* **1963**, *39*, 1397.
(85) Mealli, C.; Proserpio, D. M. *J. Chem. Educ.* **1990**, *67*.
(86) *Amsterdam Density Functional* program, release 2000.02; Vrije Universiteit: Amsterdam, 2000.
(87) Baerends, E. J.; Ellis, D. E.; Ros, P. *Chem. Phys.* **1973**, *2*, 41.
(88) Te Velde, G.; Baerends, E. J. *J. Comput. Phys.* **1992**, *99*, 84.
(89) Fonseca Guerra, C.; Snijders, J. G.; te Velde, G.; Baerends, E. J. *J. Theor. Chem. Acc.* **1998**, *99*, 391.
(90) Te Velde, G.; Bickelhaupt, F. M.; van Gisbergen, S. J. A.; Fonseca Guerra, C.; Baerends, E. J.; Snijders, J. G.; Ziegler, T. J. *Comput. Chem.* **2001**, *22*, 931.
(91) Vosko, S. H.; Wilk, L.; Nusair, M. *Can. J. Phys.* **1980**, *58*, 1200.
(92) Becke, A. D. *J. Chem. Phys.* **1986**, *84*, 4524.
(93) Becke, A. D. *Phys. Rev. A* **1986**, *38*, 3098.
(94) Perdew, J. P. *Phys. Rev. B* **1986**, *33*, 8822.
(95) Versluis, L.; Ziegler, T. J. *J. Chem. Phys.* **1988**, *88*, 322.
(96) van Lethe, E.; Baerends, E. J.; Snijders, J. G. *J. Chem. Phys.* **1993**, *99*, 4597.
(97) van Lethe, E.; Baerends, E. J.; Snijders, J. G. *J. Chem. Phys.* **1994**, *101*, 9783.
(98) van Lethe, E.; van Leeuwen, R.; Baerends, E. J.; Snijders, J. G. *Int. J. Quantum Chem.* **1996**, *57*, 281.
(99) London, F. *J. Phys. Radium* **1937**, *27*, 397.
(100) Ditchfield, R. *Mol. Phys.* **1974**, *27*, 789.
(101) Wolinski, K.; Hinton, J. F.; Pulay, P. *J. Am. Chem. Soc.* **1990**, *112*, 8251.
(102) Friedrich, K.; Seifert, G.; Grossmann, G. Z. *Phys. D* **1990**, *17*, 45.
(103) Schreckenbach, G.; Ziegler, T. J. *J. Phys. Chem.* **1995**, *99*, 606.
(104) Schreckenbach, G.; Ziegler, T. J. *Int. J. Quantum Chem.* **1997**, *61*, 899.
(105) Schreckenbach, G.; Ziegler, T. J. *Int. J. Quantum Chem.* **1996**, *60*, 753.
(106) Wolff, S. K.; Ziegler, T. J. *J. Chem. Phys.* **1998**, *109*, 895.
(107) Wolff, S. K.; Ziegler, T. J.; van Lethe, E.; Baerends, E. J. *J. Chem. Phys.* **1999**, *110*, 7689.
(108) Frisch, M. J. T., G. W.; Schlegel, H. B.; Scuseria, G. E.; Robb, M. A.; Cheeseman, J. R.; Zakrzewski, V. G.; Montgomery, Jr., J. A.; Stratmann, R. E.; Burant, J. C.; Dapprich, S.; Millam, J. M.; Daniels, A. D.; Kudin, K. N.; Strain, M. C.; Farkas, O.; Tomasi, J.; Barone, V.; Cossi, M.; Cammi, R.; Mennucci, B.; Pomelli, C.; Adamo, C.; Clifford, S.; Ochterski, J.; Petersson, G. A.; Ayala, P. Y.; Cui, Q.; Morokuma, K.; Malick, D. K.; Rabuck, A. D.; Raghavachari, K.; Foresman, J. B.; Cioslowski, J.; Ortiz, J. V.; Stefanov, B. B.; Liu, G.; Liashenko, A.; Piskorz, P.; Komaromi, I.; Gomperts, R.; Martin, R. L.; Fox, D. J.; Keith, T.; Al-Laham, M. A.; Peng, C. Y.; Nanayakkara, A.; Gonzalez, C.; Challacombe, M.; Gill, P. M. W.; Johnson, B.; Chen, W.; Wong, M. W.; Andres, J. L.; Gonzalez, C.; Head-Gordon, M.; Replogle, E. S.; Pople, J. A. *Gaussian 98*, revision A.5; Gaussian, Inc.: Pittsburgh, PA, 1998.